LETTER

doi:10.1038/nature14107

SLC38A9 is a component of the lysosomal amino acid sensing machinery that controls mTORC1

Manuele Rebsamen[1], Lorena Pochini[2], Taras Stasyk[3], Mariana E. G. de Araújo[3], Michele Galluccio[2], Richard K. Kandasamy[1], Berend Snijder[1], Astrid Fauster[1], Elena L. Rudashevskaya[1]†, Manuela Bruckner[1], Stefania Scorzoni[1], Przemyslaw A. Filipek[3], Kilian V. M. Huber[1], Johannes W. Bigenzahn[1], Leonhard X. Heinz[1], Claudine Kraft[4], Keiryn L. Bennett[1], Cesare Indiveri[2], Lukas A. Huber[3] & Giulio Superti-Furga[1]

Cell growth and proliferation are tightly linked to nutrient availability. The mechanistic target of rapamycin complex 1 (mTORC1) integrates the presence of growth factors, energy levels, glucose and amino acids to modulate metabolic status and cellular responses[1–3]. mTORC1 is activated at the surface of lysosomes by the RAG GTPases and the Ragulator complex through a not fully understood mechanism monitoring amino acid availability in the lysosomal lumen and involving the vacuolar H^+-ATPase[4–8]. Here we describe the uncharacterized human member 9 of the solute carrier family 38 (SLC38A9) as a lysosomal membrane-resident protein competent in amino acid transport. Extensive functional proteomic analysis established SLC38A9 as an integral part of the Ragulator–RAG GTPases machinery. Gain of SLC38A9 function rendered cells resistant to amino acid withdrawal, whereas loss of SLC38A9 expression impaired amino-acid-induced mTORC1 activation. Thus SLC38A9 is a physical and functional component of the amino acid sensing machinery that controls the activation of mTOR.

Amino acids are essential for mTORC1 activity, as growth factors cannot efficiently activate mTOR in their absence[5,9]. Notwithstanding the growing number of proteins involved in the activation of mTOR at the lysosomal surface, the molecular nature of the amino acid sensing mechanisms have remained elusive[1,2,4,9–13]. Several members of the solute carrier (SLC) group belonging to families capable of transporting amino acids at the plasma membrane have been shown to regulate mTOR activity[14], raising the possibility that SLCs may also be involved in the lysosomal sensing. We hypothesized the existence of an ubiquitously expressed SLC belonging to a family competent for amino acid transport[15] with a subcellular localization compatible with lysosomal amino acid sensing. Among the list of SLCs robustly expressed in two different cell lines, we focused on member 9 of the SLC38 family as it was completely uncharacterized, showed vesicular staining[16] and had been associated to lysosomes by proteomic analysis[17] (Extended Data Fig. 1a). The SLC38 family contains eleven members, and is part of a phylogenetic cluster of amino acid transporters comprising the SLC32 and SLC36 families[18] (Extended Data Fig. 1b). SLC38A9 is predicted to encompass eleven transmembrane helices and a 120-residue cytoplasmic amino-terminal region. Treatment with peptide-*N*-glycosidase (PNGase) F showed that SLC38A9 is highly glycosylated and enabled detection of the endogenous protein (Extended Data Fig. 2a, b). Supporting a possible role in growth regulatory pathways, silencing of SLC38A9 by short hairpin RNA (shRNA) in HEK293T cells resulted in a reduction of cell size and cell proliferation (Extended Data Fig. 2c, d).

To test whether SLC38A9 would associate with the complex regulating mTORC1, we engineered HEK293 cells to express tagged SLC38A9 in an inducible fashion and verified the localization of the protein to lysosomes (Extended Data Fig. 3a–c). We purified endogenously assembled protein complexes using tandem affinity purification (TAP) coupled to one-dimensional gel-free liquid chromatography tandem mass spectrometry (LC–MS/MS). The gel-free approach was critical as upon boiling SLC38A9 formed insoluble aggregates that failed to enter sodium dodecyl sulfate–polyacrylamide gels (SDS–PAGE; Extended Data Fig. 2e, f). The analysis identified all the five members of the Ragulator/LAMTOR complex and the four RAG GTPases (known as RAGA–D or RRAGA–D) as specific interactors of SLC38A9 (Fig. 1a, Extended Data Fig. 3d). Such collective high sequence coverage of all components of the Ragulator–RAG GTPases complex strongly indicated that SLC38A9 was an additional uncharacterized member. When co-expressed in HEK293T cells, SLC38A9 co-immunoprecipitated with LAMTOR1 and overexpressed LAMTOR1 bound endogenous SLC38A9 (Fig. 1b, c). We validated complex membership entirely at the endogenous level in different cell lines. Immunoprecipitation of SLC38A9 resulted in the specific recruitment of endogenous RAGA and LAMTOR1 and, conversely, immunoprecipitated RAGA bound SLC38A9 (Fig. 1d). This association was not observed when SLC38A9 was silenced, confirming specificity. Association of endogenous SLC38A9 and RAGA was demonstrated in HeLa and K562 cells (Fig. 1e, f) and in murine NIH/3T3 fibroblasts and RAW 264.7 macrophages (Extended Data Fig. 2g, h). To further challenge specificity, we applied the identical proteomic strategy to the two highest expressed members of the SLC38 family, SLC38A1 and SLC38A2, and SLC36A1 (also known as PAT1), which has been previously associated with the Ragulator–RAG GTPase complex[19]. Despite very high bait recovery, none of the Ragulator–RAG GTPase complex members was identified among the interactors, highlighting that the association of SLC38A9 with this complex is a unique property of this family member (Extended Data Fig. 3d). Moreover, when we immunoprecipitated SLC38A9, SLC38A1, SLC38A2, SLC36A1 as well as a lysosomal member of the SLC38 family, SLC38A7 (ref. 20) and a second member of the SLC36 family, SLC36A4 (also known as PAT4), only SLC38A9 co-immunoprecipitated endogenous LAMTOR1, LAMTOR3, RAGA and RAGC, with both low and high expression levels (Fig. 1g).

Immunostaining of tagged SLC38A9 in HeLa cells revealed extensive colocalization with the late endosome/lysosome markers LAMP1, CD63 and the late endosome/multivesicular bodies lipid LBPA, but not with early endosome (EEA1) or Golgi (giantin) markers (Fig. 1h–j, Extended Data Fig. 4a, b). This supports SLC38A9 being a lysosomal component of the Ragulator–RAG GTPase complex.

Full membership to this multiprotein complex would entail physical association with any of the several detected members in reciprocal purifications. We performed affinity purification coupled to mass spectrometry analysis with LAMTOR1, 3, 4 and 5, as well as RAGA and RAGC GTPases. At the core of the interacting network obtained by combining the six independent purifications we found all the expected members of the Ragulator–RAG GTPases complex, RAPTOR as well as SLC38A9 (Fig. 2a, Extended Data Fig. 5a). The overall low sequence

[1]CeMM Research Center for Molecular Medicine of the Austrian Academy of Sciences, 1090 Vienna, Austria. [2]Department DiBEST (Biology, Ecology and Earth Sciences), University of Calabria, 87036 Arcavacata di Rende, Italy. [3]Biocenter, Division of Cell Biology, Innsbruck Medical University, 6020 Innsbruck, Austria. [4]Max F. Perutz Laboratories, University of Vienna, 1030 Vienna, Austria. †Present address: Institute of Medical Chemistry, Medical University of Vienna, 1090 Vienna, Austria.

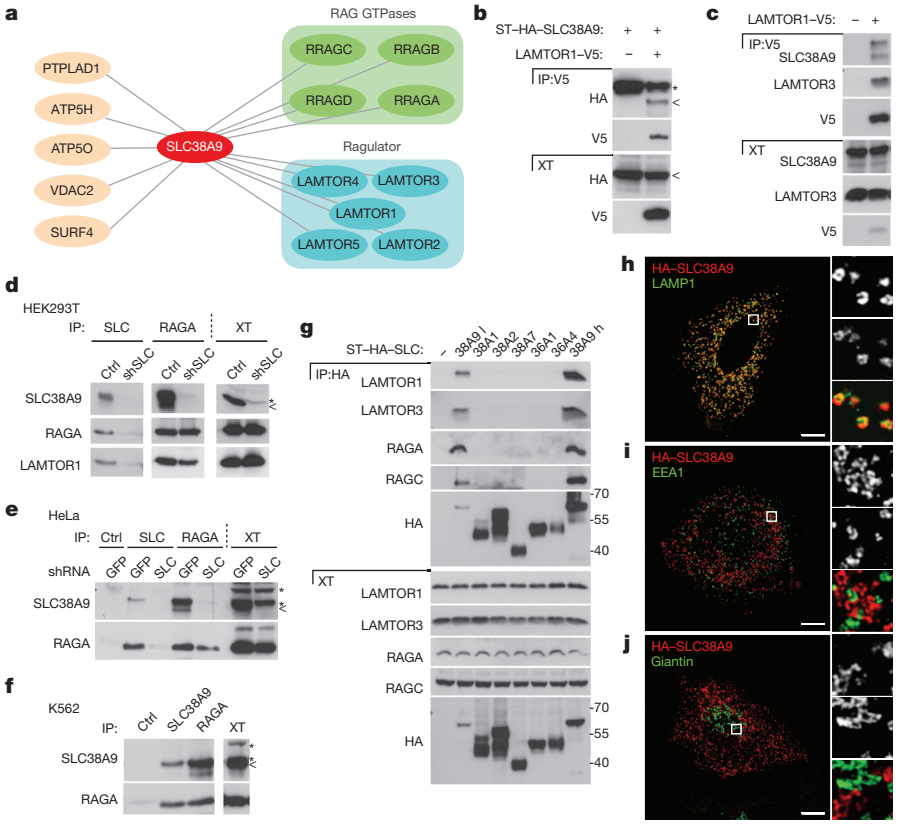

Figure 1 | SLC38A9 is a lysosomal component of the amino acid sensing machinery controlling mTORC1. **a**, Interactors of SLC38A9 identified by TAP–LC–MS/MS. Data shown are based on two independent experiments ($n = 2$), each analysed in two technical replicates. **b**–**g**, Lysates from HEK293T cells transfected with the indicated tagged constructs or empty vector (−) (**b**, **c**, **g**), control (empty vector or shGFP) or shSLC38A9-transduced HEK293T (**d**) and HeLa (**e**), or K562 (**f**) cells were subjected to immunoprecipitation. PNGase-treated immunoprecipitates (IP) and protein extracts (XT) were analysed by immunoblot with the indicated antibodies. Results are representative of two independent experiments ($n = 2$). <, ST-HA-SLC38A9; *, non-specific band. HA, haemagglutinin; ST, streptavidin; V5, V5 epitope tag. **h**–**j**, Confocal microscopy images of HeLa cells transfected with tagged SLC38A9 construct and immunostained with anti-HA and LAMP1 (**h**), EEA1 (**i**) or giantin (**j**) antibodies. Representative cells are shown. Scale bar, 10 μm.

coverage of SLC38A9 could be ascribed to inefficient proteolytic cleavage of the inaccessible transmembrane portions of the protein as it mirrored the coverage obtained when SLC38A9 was used as bait (Extended Data Fig. 5b, c). The interaction of endogenous SLC38A9 with all baits was confirmed by immunoprecipitation (Fig. 2b, c). The quality of the proteomic survey was also indicated by detection of the subunit VA0D1 of the v-ATPase complex[7] and the FLCN–FNIP2 complex[11]. Interestingly, we did not detect any other SLC member of the amino acid transporter families in any of the purifications with the members of Ragulator/GTPases complex, indicating that SLC38A9 is, at least in this cellular system, the only prominently interacting SLC.

Deletion studies indicated that the N-terminal cytoplasmic tail of SLC38A9 (amino acids 1–112), devoid of any transmembrane region, was sufficient and required to bind the Ragulator–RAG GTPases complex,

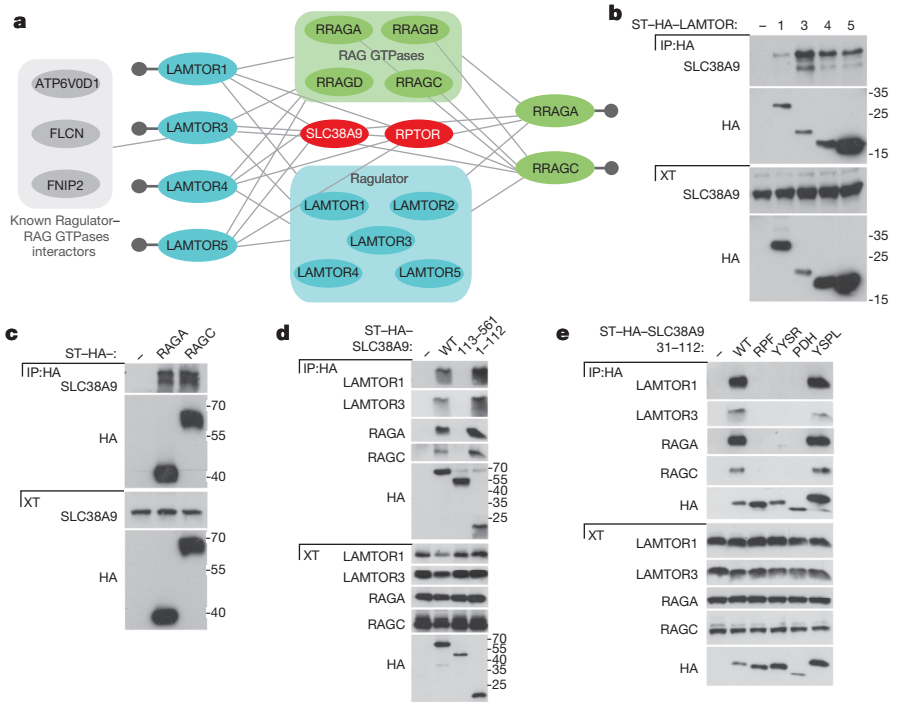

Figure 2 | SLC38A9 is an integral component of the Ragulator–RAG GTPases machinery. **a**, Interactors of LAMTOR1, LAMTOR3, LAMTOR4, LAMTOR5, RAGA and RAGC were identified by TAP–LC–MS/MS. Proteins that interacted with all the bait proteins are shown, with the addition of RAGD that was not detected in RAGC pull-down. Previously published interactors of the Ragulator–RAG GTPases complex detected are indicated. Data shown are based on two independent experiments for each condition ($n = 2$), each analysed in two technical replicates. **b**–**e**, HEK293T cells were transfected with the indicated tagged constructs or empty vector (−). Immunoprecipitates and cell extracts were treated with PNGase and analysed by immunoblot. SLC38A9 mutant constructs are labelled with the number of the encoded amino acids (**d**) or with the amino acid motif substituted to alanine (**e**). Results are representative of two independent experiments ($n = 2$). Long exp., long exposure. WT, wild type.

whereas this interaction was completely lost when the remaining eleven transmembrane-containing region (113–561), which retains lysosomal localization, was used (Fig. 2d, Extended Data Fig. 4c, d). We further mapped the minimal interacting region to amino acids 31–112 and identified four conserved motifs in this portion (Extended Data Fig. 6a, b). Mutation of any of the first three motifs completely abolished binding, while disruption of the fourth had no effect (Fig. 2e, Extended Data Fig. 6c). Importantly, none of the described mutations affected lysosomal targeting of SLC38A9 (Extended Data Fig. 4e–h). Whereas the N-terminal cytoplasmic region is evolutionarily conserved across SLC38A9 proteins, we could not detect any significant homology with the N-terminal region of any other SLC38 family member. These results defined the unique cytoplasmic portion of SLC38A9 as responsible for the interaction with the lysosomal mTOR-activating machinery.

SLC38 family members are commonly competent for the transport of glutamine[18,20] which, together with leucine and arginine, are considered the main amino acids involved in the regulation of mTORC1[9,14,21]. We monitored the transporter competence of SLC38A9 towards these amino acids in liposomes reconstituted with purified recombinant SLC38A9 (Extended Data Fig. 7a). In proteoliposomes, the cytoplasmic tail was located at the outside face of the vesicles, corresponding to the orientation observed in lysosomes (Extended Data Fig. 7b). Addition of [^{3}H]glutamine resulted in a time-dependent transport (Fig. 3a) that required intraliposomal sodium, but not addition of external sodium, and was most active at acidic pH (pH 5.5–6.5) (Extended Data Fig. 7c and e, not shown), consistent with the lysosomal localization of the natural protein. Moreover, point mutation of the putative sodium-binding site (N128A)[22] moderately affected transport (Extended Data Fig. 7d). Membrane potential artificially created by potassium gradients in the presence of valinomycin[23] both positive outside or inside did not influence the transport activity of SLC38A9 (not shown). Competition experiments showed that some polar amino acids were capable of competing efficiently for glutamine transport whereas MeAIB, an inhibitor of system A SLC38 family members, had no effect (Fig. 3b, Extended Data Fig. 7f). Direct transport assays further revealed SLC38A9 competence for [^{3}H]arginine and [^{3}H]asparagine, but not for [^{3}H]leucine or [^{3}H]histidine (Fig. 3c). The low ability of arginine to compete with glutamine transport, as previously reported also for SLC38A7 (ref. 20), may reflect differences in binding and/or transport properties for the two amino acids. The initial uptake rate calculated for 10 μM glutamine was 0.42 ± 0.10 nmol mg^{-1} of protein per minute, which is moderate when compared to other reconstituted transporters[23]. If a physiological role of SLC38A9 is to assess the intralysosomal availability of amino acids, then it is also relevant to measure its efflux-enabling activity. We monitored efflux of [^{3}H]glutamine from proteoliposomes and measured a rate of 1.7 ± 0.30 nmol mg^{-1} min^{-1} (Fig. 3d), which is higher than the uptake but overall still lower than several other amino acid transporters measured with the same approach[23]. This suggests that SLC38A9 may be a low-capacity transporter similar to SLC38A7 (ref. 20) and resembling the properties of amino acid sensors described in yeast[24] and *Drosophila*[25].

The ability of RAG GTPase heterodimers to recruit mTOR by binding Raptor is critically dependent on the nucleotide loading status and the resulting conformation of the two GTPase partners[5]. By immunoprecipitating different combinations of RAGA/B–RAGC nucleotide-binding mutant heterodimers we could recapitulate the regulated interactions with RAPTOR and LAMTOR proteins[8,11] and observed that SLC38A9 binding to RAG GTPases was markedly influenced by their

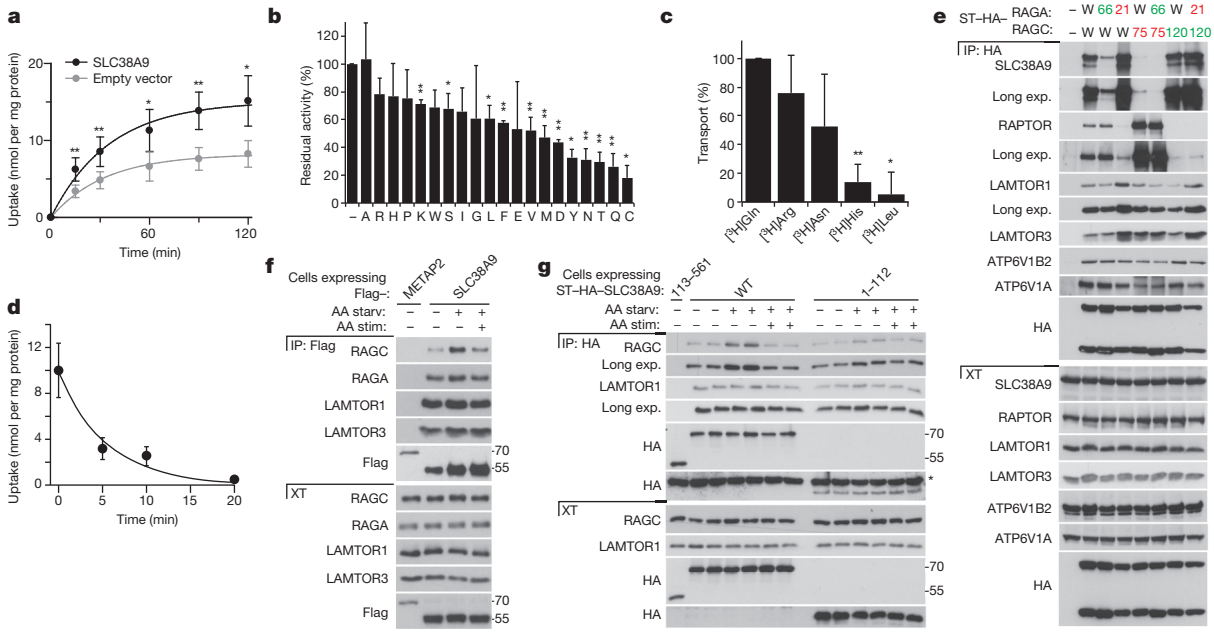

Figure 3 | SLC38A9 transports amino acids and interacts with the RAG GTPases in a nucleotide-loading and amino-acid-sensitive manner. **a**, Time course of [^{3}H]glutamine uptake in proteoliposomes reconstituted with purified SLC38A9 or with control empty vector. Values represent means ± s.d. from eight different experiments ($n = 8$). **b**, Inhibition by amino acids of [^{3}H]glutamine uptake in proteoliposomes. Values represent means of residual activity with respect to control (without added competitor) ± s.d. from three independent experiments ($n = 3$). **c**, Uptake of the indicated [^{3}H]-labelled amino acids by SLC38A9 in proteoliposomes. Values represent means of per cent in respect to glutamine transport measured in the same experiment ± s.d. from three independent experiments ($n = 3$). **d**, Time course of glutamine efflux from proteoliposomes reconstituted with SLC38A9. Values represent means of specific transport ± s.d. from three independent experiments ($n = 3$). **e**, HEK293T cells were transfected with the indicated combination of tagged RAG GTPases mutant constructs or empty vector (−). PNGase-treated immunoprecipitates and cell extracts were analysed by immunoblot. W, wild type; 66, Q66L; 21, T21N; 75, S75N; 120, Q120L. **f**, **g**, HEK293T cells stably expressing the indicated constructs were starved for amino acids and serum for 50 min (AA starv +) and stimulated with amino acids for 20 min (AA stim +). Immunoprecipitates and cell extracts were analysed by immunoblot. In **g** results of two biological replicates are shown. *, IgG light chain. Results are representative of two (**e**, **f**, $n = 2$) or three (**g**, $n = 3$) independent experiments. In **a**–**c** significance was estimated by Student's *t*-test (*$P < 0.01$ or **$P < 0.001$).

mutational state, even more than what was observed for the Ragulator complex (Fig. 3e, Extended Data Fig. 8). The low-affinity nucleotide-binding mutants RAGA(T21N) and RAGB(T54N) showed a strong increase in SLC38A9 recruitment, contrasting with the behaviour of RAGC(S75N) that abolished the binding of SLC38A9 to the heterodimer. GTP-bound RAGA(Q66L)/RAGB(Q99L) mutants showed also reduced SLC38A9 binding (Fig. 3e, Extended Data Fig. 8). These results indicate that the interaction of SLC38A9 with the critical GTPases moieties of the complex is highly conformation-specific. In cells stably expressing tagged SLC38A9, amino acid starvation strengthened the interaction between SLC38A9 and endogenous RAGC and, to a minor extent, RAGA, without significantly affecting LAMTOR1 and LAMTOR3 recruitment (Fig. 3f). Similarly, amino acid stimulation reduced the amount of recruited RAGC and RAGA. Altogether, the amino-acid-sensitive character of these binding properties are evocative of the ones exerted by Ragulator[8] and Folliculin[11] and point to a possible function of SLC38A9 in modulating the nucleotide status of the RAG GTPases. Amino acid sensitivity required the transmembrane region, as the recruitment of RAGC by the N-terminal region alone was not affected by amino acid availability (Fig. 3g). This is consistent with the notion that the eleven transmembrane helices-encompassing region is the moiety physically engaging amino acids and required to convey sensitivity.

Withdrawal of amino acids results in rapid inactivation of mTORC1. Cells stably expressing SLC38A9 showed sustained mTORC1 activation upon amino acid starvation, as monitored by the phosphorylation of the substrates S6 kinase and ULK1 (Fig. 4a, Extended Data Fig. 9a). This resulted in a delayed and reduced induction of autophagy upon amino acid starvation, as shown by quantification of LC3B relocalization to autophagosomes (Fig. 4b, Extended Data Fig. 9b), as well as sustained phosphorylation and delayed nuclear translocation of the transcription factor TFEB[26] (Extended Data Fig. 9c). Sustained mTOR activity triggered by SLC38A9 expression during starvation was inhibited by Torin 1 (Extended Data Fig. 9e). In contrast, the v-ATPase inhibitor concanamycin A had no effect in this setting, whereas it efficiently blocked mTORC1 activation induced by amino acid stimulation (Extended Data Fig. 9e, f). This suggests that the v-ATPase complex and SLC38A9 concur in the control of mTORC1 activity by amino acids. Most likely, the high expression levels of SLC38A9 resulted in an active signalling state that bypasses the v-ATPase input. Indeed, expression of the N-terminal region appears to be sufficient to confer prolonged mTORC1 activation, suggesting that this moiety assumes an active conformation independently of the transmembrane region (Fig. 4c, Extended Data Fig. 9d). Altogether, the data indicate that SLC38A9 is an upstream positive regulator of mTORC1 function.

Accordingly, silencing of SLC38A9 in HEK293T by shRNA resulted in a reduction of amino acid-induced mTORC1 activation (Fig. 4d). Cells left in culture for longer times manifested a weaker phenotype, possibly owing to compensatory adaptive mechanisms (not shown). We therefore silenced SLC38A9 by small interfering RNA (siRNA) and observed suppression of amino acid-induced mTORC1 activation in both HEK293T and HeLa cells with an efficiency that was comparable with knockdown of LAMTOR1 (Fig. 4f, Extended Data Fig. 10a). Depletion of SLC38A9 also impaired mTORC1 activation induced by cycloheximide, which mimics amino acid stimulation by blocking protein synthesis and thus inducing accumulation of intracellular amino acids[5] (Fig. 4e). This further suggests that SLC38A9 participates in mTORC1 activation at the lysosome rather than contributing to the import of extracellular amino acids at the plasma membrane. Moreover, SLC38A9 levels did not appear to be induced upon amino acid starvation, in contrast to several SLCs responsible for importing amino acids at the plasma membrane (Extended Data Fig. 10b, c).

Altogether, the work presented here identifies SLC38A9 as a novel integral component of the lysosomal machinery that controls mTORC1 activity in response to amino acids (Fig. 4g). SLC38A9 is the first member of the entire machinery shown to be competent for binding and transporting amino acids. As other solute carrier proteins, it should be eminently druggable[27]. We failed to observe a strong dependence on SLC38A9 in amino acid stimulation-induced mTOR lysosomal recruitment, which could be due to technical reasons or, more intriguingly, to separate, partly independent mechanisms controlling localization and activation of mTOR. Together with the adaptation observed upon prolonged SLC38A9 silencing, this suggests that additional sensing components are likely to operate in this pathway. Considering the low transport capacity and the physical association with the Ragulator–RAG

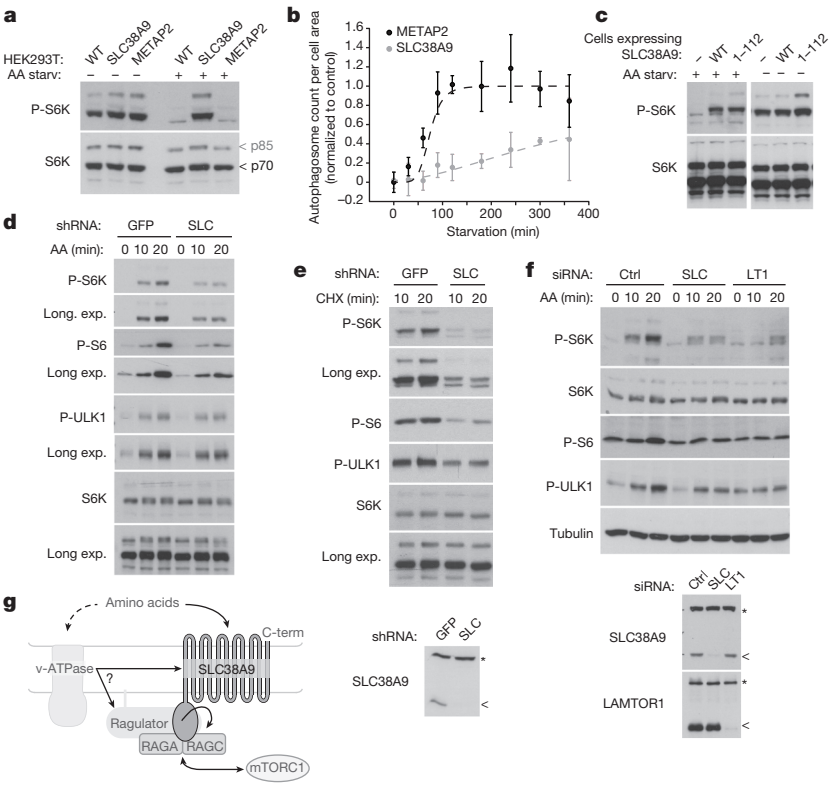

Figure 4 | SLC38A9 is a positive regulator of mTORC1 required for its activation by amino acids. **a**, Wild type, Flag–SLC38A9 or Flag–METAP2 stably expressing HEK293T cells were starved for 30 min in medium without amino acids and serum. Cell lysates were analysed by immunoblot. **b**, HEK293T cells stably expressing EGFP–LC3B and SLC38A9 or METAP2 were starved for the indicated time. LC3B-positive autophagosomes were quantified by image analysis. Data were normalized to cell size and plotted relative to the fitted METAP2 maximum. Mean ± s.d. of at least three replicate wells. **c**, HEK293T cells stably expressing the indicated untagged SLC38A9 constructs were treated and analysed as in **a**. **d**, **e**, HEK293T cells transduced with lentivirus-encoded shRNA against SLC38A9 or GFP were starved for 50 min and then stimulated with amino acids (**d**) or cycloheximide (CHX) (**e**, 25 μg ml^{-1}) for 10 or 20 min. Cell lysates were analysed by immunoblot. **f**, HEK293T were transfected with siRNA targeting SLC38A9, LAMTOR1 or non-targeting control. After 72 h, cells were treated as in **d**. In **e**, **f**, bottom panels, cell lysates were treated with PNGase; *, non-specific band. **g**, Schematic model of SLC38A9 function in amino-acid-induced mTORC1 activation. Results are representative of two (**a**–**e**, $n = 2$) or three (**f**, $n = 3$) independent experiments.

GTPase complex, it is reasonable to consider SLC38A9 a transceptor-type of SLC[24,28–30], reminiscent of yeast amino acid sensors GAP1 and ssy1p, in which amino acid engagement is used for allosteric signal transduction rather than mere transport.

Online Content Methods, along with any additional Extended Data display items and Source Data, are available in the online version of the paper; references unique to these sections appear only in the online paper.

Received 25 October 2013; accepted 20 November 2014.
Published online 7 January 2015.

1. Dibble, C. C. & Manning, B. D. Signal integration by mTORC1 coordinates nutrient input with biosynthetic output. *Nature Cell Biol.* **15,** 555–564 (2013).
2. Laplante, M. & Sabatini, D. M. mTOR signaling in growth control and disease. *Cell* **149,** 274–293 (2012).
3. Cornu, M., Albert, V. & Hall, M. N. mTOR in aging, metabolism, and cancer. *Curr. Opin. Genet. Dev.* **23,** 53–62 (2013).
4. Kim, E., Goraksha-Hicks, P., Li, L., Neufeld, T. P. & Guan, K. L. Regulation of TORC1 by Rag GTPases in nutrient response. *Nature Cell Biol.* **10,** 935–945 (2008).
5. Sancak, Y. *et al.* The Rag GTPases bind raptor and mediate amino acid signaling to mTORC1. *Science* **320,** 1496–1501 (2008).
6. Sancak, Y. *et al.* Ragulator-Rag complex targets mTORC1 to the lysosomal surface and is necessary for its activation by amino acids. *Cell* **141,** 290–303 (2010).
7. Zoncu, R. *et al.* mTORC1 senses lysosomal amino acids through an inside-out mechanism that requires the vacuolar H^+-ATPase. *Science* **334,** 678–683 (2011).
8. Bar-Peled, L., Schweitzer, L. D., Zoncu, R. & Sabatini, D. M. Ragulator is a GEF for the rag GTPases that signal amino acid levels to mTORC1. *Cell* **150,** 1196–1208 (2012).
9. Jewell, J. L., Russell, R. C. & Guan, K. L. Amino acid signalling upstream of mTOR. *Nature Rev. Mol. Cell Biol.* **14,** 133–139 (2013).
10. Bar-Peled, L. *et al.* A tumor suppressor complex with GAP activity for the Rag GTPases that signal amino acid sufficiency to mTORC1. *Science* **340,** 1100–1106 (2013).
11. Tsun, Z. Y. *et al.* The folliculin tumor suppressor is a GAP for the RagC/D GTPases that signal amino acid levels to mTORC1. *Mol. Cell* **52,** 495–505 (2013).
12. Han, J. M. *et al.* Leucyl-tRNA synthetase is an intracellular leucine sensor for the mTORC1-signaling pathway. *Cell* **149,** 410–424 (2012).
13. Panchaud, N., Peli-Gulli, M. P. & De Virgilio, C. Amino acid deprivation inhibits TORC1 through a GTPase-activating protein complex for the Rag family GTPase Gtr1. *Sci. Signal.* **6,** ra42 (2013).
14. Nicklin, P. *et al.* Bidirectional transport of amino acids regulates mTOR and autophagy. *Cell* **136,** 521–534 (2009).
15. Hediger, M. A., Clemencon, B., Burrier, R. E. & Bruford, E. A. The ABCs of membrane transporters in health and disease (SLC series): introduction. *Mol. Aspects Med.* **34,** 95–107 (2013).
16. Uhlen, M. *et al.* Towards a knowledge-based Human Protein Atlas. *Nature Biotechnol.* **28,** 1248–1250 (2010).
17. Chapel, A. *et al.* An extended proteome map of the lysosomal membrane reveals novel potential transporters. *Mol. Cell. Proteomics* **12,** 1572–1588 (2013).
18. Schiöth, H. B., Roshanbin, S., Hagglund, M. G. & Fredriksson, R. Evolutionary origin of amino acid transporter families SLC32, SLC36 and SLC38 and physiological, pathological and therapeutic aspects. *Mol. Aspects Med.* **34,** 571–585 (2013).
19. Ögmundsdóttir, M. H. *et al.* Proton-assisted amino acid transporter PAT1 complexes with Rag GTPases and activates TORC1 on late endosomal and lysosomal membranes. *PLoS ONE* **7,** e36616 (2012).
20. Hägglund, M. G. *et al.* Identification of SLC38A7 (SNAT7) protein as a glutamine transporter expressed in neurons. *J. Biol. Chem.* **286,** 20500–20511 (2011).
21. Duran, R. V. *et al.* Glutaminolysis activates Rag-mTORC1 signaling. *Mol. Cell* **47,** 349–358 (2012).
22. Zhang, Z., Gameiro, A. & Grewer, C. Highly conserved asparagine 82 controls the interaction of Na^+ with the sodium-coupled neutral amino acid transporter SNAT2. *J. Biol. Chem.* **283,** 12284–12292 (2008).
23. Oppedisano, F., Pochini, L., Broer, S. & Indiveri, C. The B degrees AT1 amino acid transporter from rat kidney reconstituted in liposomes: kinetics and inactivation by methylmercury. *Biochim. Biophys. Acta* **1808,** 2551–2558 (2011).
24. Ljungdahl, P. O. Amino-acid-induced signalling via the SPS-sensing pathway in yeast. *Biochem. Soc. Trans.* **37,** 242–247 (2009).
25. Goberdhan, D. C., Meredith, D., Boyd, C. A. & Wilson, C. PAT-related amino acid transporters regulate growth via a novel mechanism that does not require bulk transport of amino acids. *Development* **132,** 2365–2375 (2005).
26. Settembre, C. *et al.* A lysosome-to-nucleus signalling mechanism senses and regulates the lysosome via mTOR and TFEB. *EMBO J.* **31,** 1095–1108 (2012).
27. Giacomini, K. M. *et al.* Membrane transporters in drug development. *Nature Rev. Drug Discov.* **9,** 215–236 (2010).
28. Wu, B. *et al.* Competitive intra- and extracellular nutrient sensing by the transporter homologue Ssy1p. *J. Cell Biol.* **173,** 327–331 (2006).
29. Kriel, J., Haesendonckx, S., Rubio-Texeira, M., Van Zeebroeck, G. & Thevelein, J. M. From transporter to transceptor: signaling from transporters provokes re-evaluation of complex trafficking and regulatory controls. *BioEssays* **33,** 870–879 (2011).
30. Taylor, P. M. Amino acid transporters: eminences grises of nutrient signalling mechanisms? *Biochem. Soc. Trans.* **37,** 237–241 (2009).

Acknowledgements We thank D. M. Sabatini, S. Wang and Z. Tsun for discussing results before publication and generously providing Flag–SLC38A9 and Flag–METAP2 stably expressing cells, all members of the Superti-Furga laboratory for discussions, the Bennett laboratory for the proteomic analyses, F. Pauler and the Barlow laboratory for the RNA-seq analysis and M. Gstaiger for providing expression vectors. This work was supported by the Austrian Academy of Sciences, ERC grant to G.S.-F. (i-FIVE 250179), EMBO long-term and Marie Curie fellowships to M.R. (ALTF 1346-2011, IEF 301663), EMBO long-term fellowship to R.K.K. (ALTF 314-2012), Swiss NSF fellowship (P300P3_147897) to B.S., Vienna Science and Technology Fund (WWTF VRG10-001) and the Austrian Science Fund (FWF P 25522-B20) to C.K., the Italian Ministry of Instruction University and Research, PON-ricerca e competitività 2007-2013 (no. PON01_00937) to C.I., the Austrian Federal Ministry for Science and Research (GenAu projects, APP-III and BIN-III) to L.A.H., K.L.B. and G.S.-F., the Austrian Science Fund MCBO/SFB021 to L.A.H.

Author Contributions M.R. and G.S.-F. conceived the study. L.P., M.G. and C.I. designed and performed transport assays. M.R., T.S., M.E.G.d.A., E.L.R., M.B., K.L.B., L.A.H. and G.S.-F. designed and performed TAP-mass spectrometry experiments. M.R., M.E.G.d.A., B.S., A.F., M.B., S.S. and P.A.F. performed the other experiments. M.R., L.A.H. and G.S.-F. designed the other experiments. R.K.K. and B.S. performed bioinformatic data and image analysis. K.V.M.H., J.W.B., L.X.H., C.K. generated reagents and provided scientific insight. M.R. and G.S.-F. wrote the manuscript. All authors contributed to the discussion of results and participated in manuscript preparation.

Author Information The protein-protein interactions have been submitted to the IMEx (http://www.imexconsortium.org) consortium through IntAct (http://www.ebi.ac.uk/intact/) and assigned the identifier IM-23283. The SLC network has the IntAct accession number EBI-9975668 and the RAGA-RAGC-LAMTOR network is EBI-9975664. RNA-Seq data is available in ArrayExpress (http://www.ebi.ac.uk/arrayexpress) under the accession number E-MTAB-3102. Reprints and permissions information is available at www.nature.com/reprints. The authors declare competing financial interests: details are available in the online version of the paper. Readers are welcome to comment on the online version of the paper. Correspondence and requests for materials should be addressed to G.S.-F. (gsuperti@cemm.oeaw.ac.at).

METHODS

Antibodies. Antibodies used were against SLC38A9 (HPA043785 Sigma), LAMTOR1 (8975 Cell Signaling), LAMTOR3 (8169 Cell Signaling), RAGA (4357 Cell Signaling), RAGC (5466 Cell Signaling), phospho-p70 S6 Kinase (Thr389) (9234 Cell Signaling), phospho-S6 (Ser240/244) (2215 Cell Signaling), phospho-ULK1 (Ser757) (6888 Cell Signaling), raptor (2280 Cell Signaling), ATP6V1B2 (ab73404 Abcam), ATP6V1A (GTX110815 GeneTex), mouse anti-rabbit IgG (conformation-specific) (3678 Cell Signaling), LAMP1 (555798 Pharmingen and ab25630 Abcam), LAMP2 (sc-18822 Santa Cruz), CD63 (H5C6 DSHB), LBPA (Z-PLBPA Echelon, Tebu-bio), EEA1 (sc33585 Santa Cruz), giantin (ab24586 Abcam), p70 S6 kinase (sc-230 Santa Cruz), ULK1 (8054 Cell Signaling), tubulin (ab7291 Abcam), RCC1 (sc55559 Santa Cruz), HA (H6533 Sigma, 3724 Cell Signaling, MMS-101P Covance or sc-805 Santa Cruz), V5 (ab9116 Abcam), His (A7058 Sigma), Flag (F7425 Sigma). The secondary antibodies used were goat anti-mouse AlexaFluor568 (A-11004 and A-11031 Molecular probes), goat anti-rabbit AlexaFluor568 (A-11036 Molecular probes), goat anti-mouse AlexaFluor488 (A-11001 Molecular probes), goat anti-rabbit AlexaFluor488 (A-11008 Molecular probes) and horseradish peroxidase (HRP)-conjugated antibodies (Jackson ImmunoResearch).

Plasmids. Expression constructs were generated by PCR amplification from EST or from plasmids obtained from Addgene (RAGA: Plasmid 19298 (WT) and 19300 (Q66A); RAGB: 19301 (WT) and 19303 (Q99A); RAGC: 19304; EGFP–LC3B: 11645) or from the Harvard Medical School plasmid repository (SLC38A1, SLC38A2, SLC38A7, SLC36A1, SLC36A4) and subcloned by Gateway cloning (Invitrogen) into pTRACER-CV5-GW or pTO-SII-HA-GW[31] with N-terminal tagging for SLC38A9, SLC38A1, SLC38A2, SLC38A7, SLC36A1, SLC36A4, RAGA, RAGB, RAGC and LAMTOR3 (human and mouse) and C-terminal tagging for LAMTOR1, 4 and 5. Point mutations were introduced by site-directed mutagenesis (InvivoGen).

Cells. HEK293T, Raw264.7, NIH/3T3 and K562 cells were obtained from ATCC and DMSZ. HeLa were provided by M. Hentze. HEK293 Flp-In TREx cells that allow doxycycline-dependent transgene expression were from Invitrogen. Cells were kept in DMEM (Sigma) or RPMI medium (PAA Laboratories) supplemented with 10% (v/v) FBS (Invitrogen) and antibiotics (100 U ml^{-1} penicillin and 100 mg ml^{-1} streptomycin) and checked for mycoplasma by PCR or ELISA.

Transfections, cell lysis, deglycosylation, immunoprecipitations and fractionation. Cells were transfected with Polyfect (Qiagen) and used for experiments after 24 h. For lysis, cells were resuspended in Nonidet-40 lysis buffer (1% NP-40, 50 mM HEPES pH 7.4, 250 mM NaCl, 5 mM EDTA, Halt phosphatase inhibitor cocktail (ThermoScientific), one tablet of EDTA-free protease inhibitor (Roche) per 50 ml) on ice for 5 min. Lysates were cleared by centrifugation in a microcentrifuge (13,000 r.p.m., 10 min, 4 °C). Proteins were quantified with BCA (Pierce). For immunoprecipitations, lysates were precleared on Sepharose6 beads (Sigma) (40 min with rotation, 4 °C) and then incubated either with HA-, V5- or Flag-coupled beads (3 h with rotation, 4 °C) or with primary antibody and protein G-sepharose (GE healthcare) (14 h with rotation, 4 °C). Beads were recovered and washed four times with lysis buffer before analysis by SDS–PAGE and immunoblotting. When required, a mouse anti-rabbit IgG (conformation specific) antibody was used for immunoblot and revealed with an anti-mouse HRP-conjugated antibody to avoid detection of immunoglobulin heavy chains. In case of detection of endogenous SLC38A9, samples were treated with PNGase (NEB, 250 U for 30 µl, 1 h, 37 °C) before SDS–PAGE. Nuclear-cytoplasm cell fractionation was performed as previously described[32].

Generation of stably expressing cells. HEK293T cells expressing codon-optimized Flag-tagged SLC38A9 isoform 1 (GenScript) were generated using a modified pLKO.1 lentiviral vector having a CMV promoter (pLJM60). Lentiviruses were produced by co-transfection of the lentiviral transfer vector with the ΔVPR envelope and CMV VSV-G packaging plasmids into HEK293T cells using the XTremeGene 9 transfection reagent (Roche). The media was changed 24 h post-transfection to DMEM supplemented with 30% IFS. Virus-containing supernatants were collected 48 and 72 h after washing, filtered and used for spin infection (2,200 r.p.m. for 1 h) of target HEK293T cells in presence of 8 µg ml^{-1} polybrene. 24 h after infection, the virus was removed and the cells selected with puromycin. HEK293T expressing codon-optimized untagged or ST-HA-tagged SLC38A9 (GenScript) full length, C-terminal (113–561) or N-terminal region (1–112) were generated using a modified pMSCV retroviral vector. Cells expressing EGFP-LC3B or TFEB-STHA were generated by infecting Flag–SLC38A9 or Flag–METAP2 stable cells using a modified pMSCV retroviral vector and blasticidin selection.

RNAi. For shRNA-mediated knockdown, shRNA-encoding pLKO.1 targeting SLC38A9 (ThermoFisher, TRCN0000151238) or GFP (ThermoFisher, RHS4459) were used. Lentiviruses were produced using second-generation packaging plasmids pMD2-VSVG and pCMV-R8.91. HEK293T cells were co-transfected with packaging plasmids and the shRNA-encoding plasmids. Cells were washed 16 h after transfection. Virus-containing supernatants were collected 24 h after washing, filtered and used for infection. After 48 h of infection, HEK293T cells were selected with puromycin (4 µg ml^{-1}) and used for experiments from 3 to 7 days later. For siRNA-mediated knockdown, HEK293T cells were transfected with Lipofectamine RNAiMAX (Invitrogen) with 30 nM of siRNA pool; HeLa with HiPerfect (Qiagen) with 60 nM of siRNA pool. After 48 h cells were seeded and subjected 24 h later to amino acid stimulation as described. ON-TARGETplus SMARTpool against SLC38A9 (L-007337-02, target sequences: ACACUGAAGGAUACGGUAA, GAUCCUGGACCUAUGAAUA, GAAGAGUGCUAUGUGUAUA, CAUGUCAUUCAGAGGGUUA), LAMTOR1 (L-020916-02, target sequences: UCUCCAGGAUAGCUGCUUA, GGCUUAUACAGUACCCUAA, AAGUGAGGGUAGAACCUUU, GUUUGUCACCCUCGAUAAA) and non-targeting pool (D-001810-10) were from ThermoScientific.

Proteomics. Flp-in HEK293 T-Rex cell lines inducibly expressing ST-HA-tagged SLC38A9, SLC38A1, SLC38A2, SLC36A1, RAGA, RAGC, GFP or LAMTOR complex subunits were generated as described[33]. Tandem affinity STREP-HA purifications were performed as previously described[31]. In brief, cells were stimulated with doxycycline/tetracycline for 24 h to induce expression of ST-HA-tagged bait proteins. LAMTOR3 pull-downs were done using murine protein version and performed after 9 h starvation in serum-free medium. Protein complexes were isolated by TAP using streptavidin agarose followed by elution with biotin, and a second purification step using HA–agarose beads. Proteins were eluted with 100 mM formic acid, neutralized with triethylammonium bicarbonate (TEAB) and digested with trypsin, and the peptides were analysed by LC–MS/MS.

MS data analysis and interaction data filtering. Peak list data were extracted from RAW files using ProteoWizard (release 3.0.3201, http://proteowizard.sourceforge.net/) and searched against human SwissProt database version v2013.01_20130110 (37,261 sequences and common contaminants). The search engines MASCOT (v2.3.02, MatrixScience, London, UK) and Phenyx (v2.5.14, GeneBio, Geneva, Switzerland)[34] were used. The searches were submitted to MASCOT using in-house perl scripts at precursor and fragment ions mass tolerances ± 10 p.p.m. and ± 0.6 Da, respectively. Using the high-confidence identifications from this search, precursor and fragment ion masses were recalibrated for a second-pass search on MASCOT and Phenyx with precursor and fragment ions mass tolerances ± 4 p.p.m. and ± 0.3 Da, respectively. One tryptic missed-cleavage was permitted. Carbamidomethyl cysteine and oxidized methionine were set as fixed and variable modifications, respectively. A false discovery rate of $<0.25\%$ and $<0.1\%$ were used for proteins and peptides, respectively, as described[35]. SAINT AP-MS filtering software[36] was used to filter the interactions using GFP TAP as negative control. All prey proteins with a SAINT AvgP of >0.95 were identified as high-confidence interactors. In addition, proteins with a spectral count of 1 or a CRAPome[37] frequency of >0.1 were excluded. For the LAMTOR-RAG network, we retained only those proteins that interacted with all the bait proteins (RAGD was not detected in RAGC pull-down).

Immunofluorescence. HEK293T cells were plated on fibronectin-coated glass coverslips and, after 16 h, induced with doxycycline. After 24 h, cells were washed with PBS, fixed (PBS, 4% formaldehyde) and permeabilized (PBS, 0.3% saposin, 10% FBS). Slides were incubated with anti-HA (sc-805 Santa Cruz), anti-LAMP1 (ab25630 Abcam) or anti-LAMP2 (sc-18822 Santa Cruz) antibodies (1 h, 25 °C, PBS, 0.3% saposin, 10% FBS). After three washes slides were incubated with goat anti-mouse AlexaFluor568 or anti-rabbit AlexaFlour488 antibodies (Invitrogen, 1 h, 25 °C, PBS, 0.3% saposin, 10% FBS). After DAPI staining, slides were washed three times and mounted on coverslips with ProLong Gold (Invitrogen). Images were taken with a Zeiss Laser Scanning Microscope (LSM) 700. Images were exported from lsm files to tiff files, and analysed using custom Matlab code. Nuclei and cell outlines were detected based on the DAPI and combined immunofluorescence stains respectively, and colocalization measurements were restricted to cytoplasmic regions. Colocalization was measured as the percentage of SLC38A9 (green) pixel values above background that are also above background in the LAMP1 or LAMP2 (red) channel. The SLC38A9 and LAMP1 or LAMP2 colocalization was verified to be robust to variations in the background threshold, and also shows up as significant pixel value correlations between the red and green channels.

HeLa cells were seeded to 80% confluency for transfection (Lipofectamine LTX, Invitrogen). 24 hours post transfection, cells were split into glass coverslips and incubated for another 24 hours. Cells were then washed with PBS and fixed in 4% PFA in cytoskeleton buffer (20 mM PIPES pH 6.8, 150 mM NaCl, 5 mM EGTA, 5 mM glucose and 10 mM $MgCl_2$). Permeabilization and blocking were preformed simultaneously by incubating the cells in cytoskeleton buffer supplemented with 0,025% saponin and 50 mM NH_4Cl. Cells were then incubated with primary antibodies diluted in blocking buffer for 2 hours at room temperature. Cells were then washed 6 times in cytoskeleton buffer supplemented with 50 mM NH_4Cl and incubated with the secondary antibodies diluted in blocking buffer for 45 min at room temperature. Upon washing 6 times in cytoskeleton buffer supplemented with 50 mM NH_4Cl, the coverslips were mounted using Vectashield hardening medium (vectorlabs). *Z*-stack images were taken with an SP5 Laser Scanning confocal Microscope (Leica) and a ×63x oil immersion objective (na 1.4). Original images

were deconvoluted using Huygens professional Deconvolution and Analysis Software (Scientific Volume imaging). The *Z*-stack ids files were then visualized in ImageJ (open source version), converted into a colour stack image and a representative *Z* plane was selected. The single plane images were finally converted to Adobe Photoshop CS6 format. Representative cells are shown in all figures at the same exposure and magnification.

Cell size and autophagosome measurements. HEK293T cells transduced with shRNA against SLC38A9 or GFP cells were seeded 24 h before fixation (PBS, 4% formaldehyde), permeabilized (PBS, 0.3% Saposin, 10% FBS) and stained with DAPI. Images were taken by automated microscopy using the PerkinElmer Operetta with ×20 magnification in confocal mode. Images were analysed using CellProfiler (http://www.cellprofiler.org), CellClassifier (http://www.pelkmanslab.org/?page_id=63), Population Context measurement code (https://www.pelkmanslab.org/?page_id=1150) and custom Matlab code written specifically for this study. CellProfiler was used to detect individual nuclei on each image, and iterative machine learning using CellClassifier was applied to detect properly segmented interphase nuclei. Population context measurement code was used to measure the local cell density of each individual cell, and cell size measurements were restricted to sparse cells to avoid local crowding from confounding the measurements. We used the typical nucleus diameter (that is, the diameter of a circle with the same area as that measured for each nucleus) as a robust proxy for cell size[38]. We confirmed that the cell size reduction induced by SLC38A9 shRNA treatment were present for a broad range of different local cell densities. EGFP–LC3B and SLC38A9 or METAP2 expressing cells were seeded in 96-well plates for imaging. After 24 h cells were washed with PBS and starved for amino acids and serum for the indicated time. Three by three images were acquired per well with the Operetta at ×20 magnification on living cells to minimize disruption of EGFP–LC3B-positive autophagosomes. After imaging cells were fixed, DAPI-stained and reimaged. Autophagosomes were quantified from the GFP channel using custom Matlab analysis, based on a thresholding of the integrated Laplacian of Gaussian transformation for diameters between 8 and 30 pixels. Candidate spots with a local GFP-signal enrichment of less than 42% were discarded, and remaining spots were considered autophagosomes, and normalized to the cell number and area for each condition. Each condition was measured in three replicate wells accounting for over 85,000 cells. Adjusted hill curves were fit and data were normalized to the maximum fitted value in the METAP2 control cell line.

Cell proliferation measurements. HEK293T cells transduced with shRNA against SLC38A9 or GFP were seeded and counted every 24 h using Casy (Roche).

Amino acids starvation and stimulation. HEK293T cells grown in RPMI were washed with PBS and starvation was performed by incubating the cells for 50 min in amino-acid-free RPMI without serum. Cell were then stimulated for 10 or 20 min by the addition of RPMI containing a two-time concentrated solution of amino acids. After stimulation, the final concentration of amino acids in the media was the same as in RPMI. In case of cycloheximide treatment, amino-acid-starved cells were stimulated by addition of cycloheximide diluted in amino-acid-free RPMI at a final concentration of 25 μg ml^{-1}. HeLa cells grown in RPMI were stimulated for 10 or 20 min by the addition of RPMI containing a two time concentrated solution of amino acids and insulin (1 μM final concentration, Sigma, I9278). Concanamycin A (sc202111 Santa Cruz) was used at 5 μM and torin 1 (4247, Tocris Bioscience) at 250 nM. Amino-acid-free RPMI medium powder (R8999-04A, US biological) was complemented with sodium bicarbonate and sodium phosphate, dissolved in water, adjusted to pH 7.4 and filtered. RPMI containing a two time concentrated solution of amino acids was obtained by complementing amino-acid-free RPMI medium with RPMI 1640 amino acids solution (R7131, Sigma), adjusted to pH 7.4 and filtered. L-glutamine (59202C, Sigma) was added shortly before usage.

RNA sequencing. RNA was extracted using TRI reagent (SIGMA), treated with DNase I (DNA free kit, Ambion) and RiboZero kit (Epicentre) to remove ribosomal RNA. The library was prepared using ScriptSeq kit version 1 (Epicentre, strand-specific library). Sequencing was performed on Illumina HiSeq 2000. Sequence reads in fastq format was aligned against RefSeq hg19 build (as downloaded on 2.9.2011) using TopHat and FPKM (fragments per kilobase of exon per million fragments mapped) values were calculated using Cufflinks.

qPCR. Total RNA was isolated using the RNeasy Mini Kit (Qiagen). RNA was reverse transcribed using oligo(dT) primers using RevertAid Reverse Transcriptase (Fermentas). Quantitative PCR was carried out on a RotorGene RG-600 (Qiagen) PCR machine using the SensiMix SYBR kit (Bioline). Results were quantified using the $2^{-\Delta\Delta C(t)}$ method, using GAPDH expression levels for normalization.

Primers : SLC38A9_Fw : TCCTTTGGGCAGTGGTCGAG,_Rev : ACTCCCG GCACTTGGACAAA; GAPDH_Fw : GAAGGTGAAGGTCGGAGT, Rev : GAA GATGGTGATGGGATTTC.

Cloning, expression and purification of recombinant human SLC38A9. The human SLC38A9 cDNA was optimized according to *Escherichia coli* codon usage by GenScript. In this optimized gene, the Codon Adaptation Index (CAI) was upgraded from 0.63 (wild type) to 0.87, the GC content and unfavourable peaks were optimized to prolong the half-life of the mRNA and a ribosome binding site was removed. The optimized cDNA was then sub-cloned into expression vector (pH6EX3-His_6-hSLC38A9)[39]. The plasmid was used to transform *E. coli* Lemo21(DE3)pLysS (NEB). Selection on LB-agar was performed as previously described[39]. 0.1 mM rhamnose was added to modulate RNA polymerase expression. After addition of 0.4 mM IPTG cells were grown at 39 °C for 2 h. Cells were treated as previously described[39]. The protein patterns of the cell lysate fractions were analysed by SDS–PAGE. The insoluble cell fraction (about 1.5 mg proteins) from cells expressing SLC38A9 or empty vector transfected cells, was washed with 100 mM Tris/HCl and resuspended in 100 mM β-mercaptoethanol, 3.5 M urea, 0.5% sarkosyl, 200 mM NaCl, 10% glycerol, 20 mM Tris/HCl pH 8.0 and centrifuged at 12,000*g* for 10 min at 4 °C. The resulting supernatant (about 1 ml) was applied onto a column (0.5 cm × 2.5 cm) filled with His select nickel affinity gel (Sigma) pre-conditioned with 8 ml of 0.1% sarkosyl, 200 mM NaCl, 10% glycerol, 10 mM Tris/HCl pH 8.0. The elution was performed with 10 ml of 0.1% $C_{12}E_8$, 150 mM NaCl, 10% glycerol, 5 mM DTE, 10 mM Tris/HCl pH 8.0 (washing buffer), 1.4 ml of the same buffer plus 10 mM imidazole; then the purified protein fraction (4–7 μg protein) was eluted by 1.4 ml of the same buffer plus 50 mM imidazole.

Reconstitution of SLC38A9 in proteoliposomes and transport measurements. The purified fractions from SLC38A9 or empty vector preparation were reconstituted by removing the detergent as previously described[40] with a batch-wise procedure from a mixture of 400 μl of protein (about 2 μg protein in 0.1% $C_{12}E_8$, β-mercaptoethanol 6 mM, 10% glycerol, 20 mM Tris/HCl pH 8.0, 150 mM NaCl, 50 mM imidazole), 80 μl of 10% $C_{12}E_8$, 100 μl of 10% egg yolk phospholipids (w/v), 20 mM HEPES/Tris pH 6.5. 600 μl of proteoliposomes were passed through a Sephadex G-75 column (0.7 cm diameter × 15 cm height) preequilibrated with 20 mM HEPES/Tris pH 6.5. Transport (uptake) measurement was started adding 10 μM [^{3}H]glutamine or other radioactive substrates as indicated (0.5 μCi $nmol^{-1}$) to 100 μl proteoliposomes aliquots at 25 °C. Transport was stopped by applying each sample of proteoliposomes on a Sephadex G-75 column (0.6 × 8 cm) to separate the external from the internal radioactivity. In competition experiments, the indicated amino acids (1 mM) were added together with [^{3}H]glutamine (10 μM) and transport was measured at 60 min. For efflux measurements, aliquots of the same pool of proteoliposomes passed through a Sephadex G-75 column (0.7 cm diameter × 15 cm height) preequilibrated with 20 mM HEPES/Tris pH 6.5 were incubated with external 10 μM [^{3}H]glutamine. After 120 min of loading, proteoliposomes were passed again through a Sephadex G-75 column (0.7 cm diameter × 15 cm height) preequilibrated with 20 mM HEPES/Tris pH 6.5, for removing the residual external radioactivity. The time course of [^{3}H]glutamine efflux was then measured stopping the efflux reaction at each time interval by applying proteoliposome samples on a Sephadex G-75 column (0.6 × 8 cm) to separate the external from the internal radioactivity. In both uptake and efflux assays, proteoliposomes eluted with 1 ml 50 mM NaCl were collected in scintillation cocktail for counting. The amount of reconstituted recombinant protein was estimated as previously described[39]. Time course data were interpolated by a first order rate equation from which the initial rate of transport was calculated as k x transport at equilibrium. [3,4-^{3}H(N)]L-Glutamine from PerkinElmer; [ring-2,5-^{3}H]L-histidine, [^{3}H]L-asparagine from Campro Scientific.

Orientation of SLC38A9 in proteoliposomes. After purification, His-SLC38A9 was incubated overnight at 37 °C in absence or in presence of 1 U thrombin (GE healthcare) and then assayed by immunoblotting using anti-His or anti-SLC38A9 antibody. To assess the orientation of SLC38A9, reconstituted proteoliposomes were centrifuged at 108,000*g* for 90 min, resuspended in 20 mM HEPES/Tris pH 6.5, incubated overnight at 37 °C with 1 U thrombin in the same conditions of the purified protein. After incubation proteoliposomes were dissolved by 2.5% SDS and 0.2 M Tris/HCl pH 6.8. and immunoblotting analysis was performed as described for the purified protein.

Assay of pH and intraliposomal sodium dependence of the SLC38A9 function. Reconstitution was performed in 20 mM HEPES/Tris buffer at different pH. Transport (uptake) was started by adding to proteoliposomes10 μM [^{3}H]glutamine in 20 mM HEPES/Tris buffer at the same pH of the reconstitution mixture and stopped after 30 min. To test sodium dependency, SLC38A9 was purified omitting NaCl from elution buffer. Reconstitution was performed in the absence or in the presence of 20 or 50 mM NaCl and transport (uptake) measurement was performed.

Statistical analysis. A normal distribution of data was assumed and appropriate test were applied.

31. Varjosalo, M. *et al.* Interlaboratory reproducibility of large-scale human protein-complex analysis by standardized AP-MS. *Nature Methods* **10,** 307–314 (2013).
32. Giambruno, R. *et al.* Affinity purification strategies for proteomic analysis of transcription factor complexes. *J. Proteome Res.* **12,** 4018–4027 (2013).
33. Pichlmair, A. *et al.* Viral immune modulators perturb the human molecular network by common and unique strategies. *Nature* **487,** 486–490 (2012).

34. Colinge, J., Masselot, A., Giron, M., Dessingy, T. & Magnin, J. OLAV: towards high-throughput tandem mass spectrometry data identification. *Proteomics* **3,** 1454–1463 (2003).
35. Bennett, K. L. *et al.* Proteomic analysis of human cataract aqueous humour: Comparison of one-dimensional gel LCMS with two-dimensional LCMS of unlabelled and iTRAQ(R)-labelled specimens. *J. Proteomics* **74,** 151–166 (2011).
36. Choi, H. *et al.* SAINT: probabilistic scoring of affinity purification-mass spectrometry data. *Nature Methods* **8,** 70–73 (2011).
37. Mellacheruvu, D. *et al.* The CRAPome: a contaminant repository for affinity purification-mass spectrometry data. *Nature Methods* **10,** 730–736 (2013).
38. Snijder, B. *et al.* Population context determines cell-to-cell variability in endocytosis and virus infection. *Nature* **461,** 520–523 (2009).
39. Galluccio, M. *et al.* Over-expression in *E. coli* and purification of the human OCTN1 transport protein. *Protein Expr. Purif.* **68,** 215–220 (2009).
40. Pochini, L., Scalise, M., Galluccio, M., Amelio, L. & Indiveri, C. Reconstitution in liposomes of the functionally active human OCTN1 (SLC22A4) transporter overexpressed in *Escherichia coli*. *Biochem. J.* **439,** 227–233 (2011).

a

RefSeqNT	GeneSymbol	EntrezGeneID	HEK293_FPKM	K562_FPKM	Average _FPKM	PubMed_entry
NM_001145144	SLC1A5	6510	47.08	56.21	51.65	92
NM_001013251	SLC3A2	6520	22.28	54.08	38.18	62
NM_018976	SLC38A2	54407	17.46	31.18	24.32	80
NM_001077484	SLC38A1	81539	24.41	9.34	16.87	60
NM_014331	SLC7A11	23657	9.35	7.12	8.24	148
NM_173514	SLC38A9	153129	5.81	8.83	7.32	1
NM_003045	SLC7A1	6541	9.89	2.87	6.38	81
NM_052831	SLC18B1	116843	6.10	3.68	4.89	1
NM_003038	SLC1A4	6509	1.40	7.93	4.66	36
NM_080546	SLC44A1	23446	5.85	3.10	4.48	19

b

RefSeqNT	GeneSymbol	EntrezGeneID	HEK293_FPKM	K562_FPKM
NM_001077484	SLC38A1	81539	24.41	9.34
NM_018976	SLC38A2	54407	17.46	31.18
NM_006841	SLC38A3	10991	0.05	0.00
NM_018018	SLC38A4	55089	0.01	0.00
NM_033518	SLC38A5	92745	0.03	3.22
NM_153811	SLC38A6	145389	0.99	1.90
NM_018231	SLC38A7	55238	0.92	1.49
NM_001080442	SLC38A8	146167	0.00	0.00
NM_173514	SLC38A9	153129	5.81	8.83
NM_138570	SLC38A10	124565	0.72	1.95
NM_173512	SLC38A11	151258	0.00	0.00
NM_078483	SLC36A1	206358	0.77	0.49
NM_181776	SLC36A2	153201	0.00	0.00
NM_181774	SLC36A3	285641	0.00	0.00
NM_152313	SLC36A4	120103	4.19	0.11
NM_080552	SLC32A1	140679	0.00	0.00

Extended Data Figure 1 | Expression of SLC members of amino acid transporter families. **a**, Table of SLCs belonging to amino acid transporter families robustly expressed in HEK293 and K562 cells as monitored by RNA-seq. SLC members of amino acid transporter-containing families[16] (SLC1, 6, 7, 16, 17, 18, 32, 36, 38 and 43 families) expressed (FPKM >0.5) in both cell lines were ranked according to their expression level, top ten are shown. The number of PubMed entries was obtained by querying the GeneSymbol (24 October 2013). **b**, Expression of members of the SLC32, SLC36 and SLC38 families in HEK293 and K562 cells.

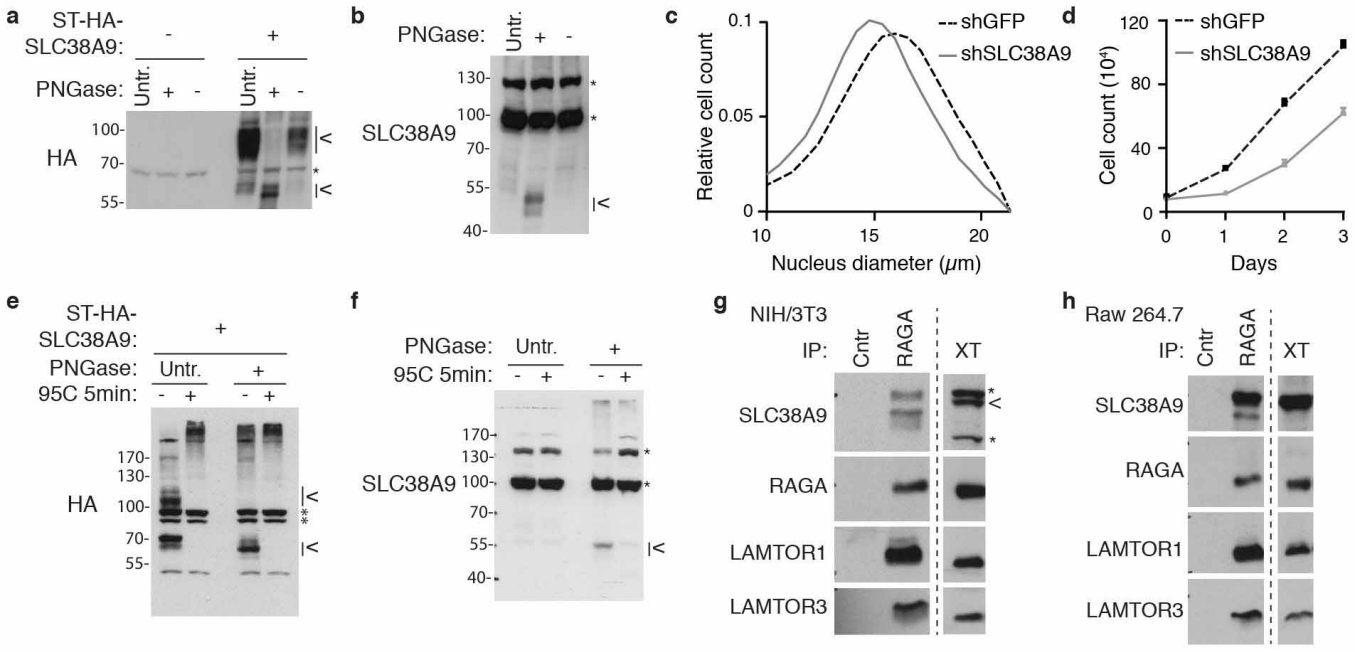

Extended Data Figure 2 | Biochemical and functional characterization of SLC38A9. **a**, **b**, Where indicated, HEK293T cells were transfected with tagged SLC38A9 constructs (+) or empty vector (−). Cell lysates were left untreated (Untr.) or incubated 1 h at 37 °C in presence or absence of PNGase and analysed by immunoblot. Results are representative of two independent experiments ($n = 2$). **c**, Cell size measurements of HEK293T cells after short hairpin (shRNA)-mediated knockdown against GFP (control, dashed black line) or SLC38A9 (grey line), measured by automated microscopy and image analysis. Sparse and interphase cells were selected using image analysis and machine learning, and nucleus diameter was used as robust proxy for cell size[38]. Smoothed distributions of 2,400 and 4,165 cells, respectively, are shown. **d**, Cell proliferation measurement of HEK293T cells transduced with lentivirus-encoded shRNA against SLC38A9 or GFP. 10^5 cells were seeded and counted every 24 h. Mean values ± s.d. from triplicates. Results are representative of two independent experiments ($n = 2$). **e**, **f**, Where indicated, HEK293T cells were transfected with tagged SLC38A9. Cell lysates were prepared and left untreated (Untr.) or incubated 1 h at 37 °C with PNGase and analysed by immunoblot, Where indicated, cell lysates were boiled for 5 min at 95 °C after PNGase treatment. **g**, **h**, Lysates from murine NIH/3T3 (**g**) or Raw 264.7 (**h**) cells were subjected to immunoprecipitation with the indicated antibodies, treated with PNGase and analysed by immunoblot. Results are representative of two independent experiments ($n = 2$). <, SLC38A9; *, non-specific band.

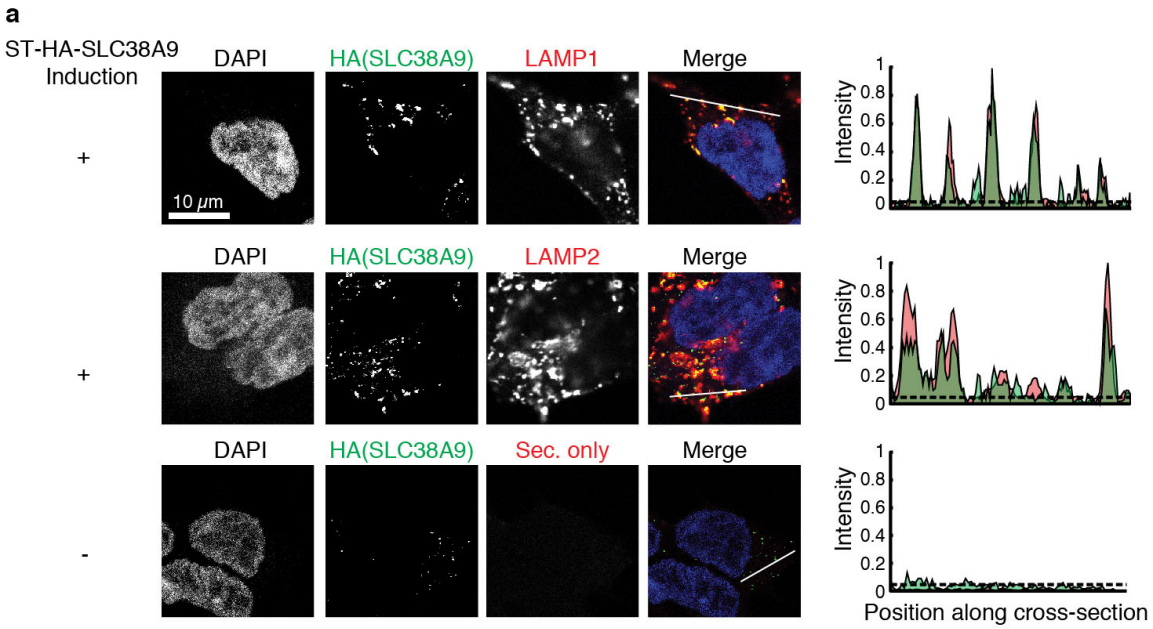

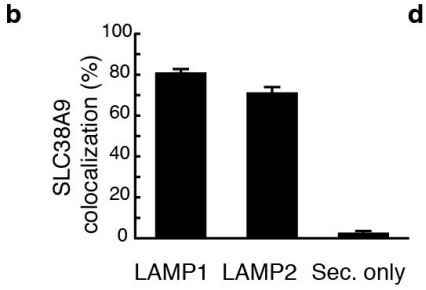

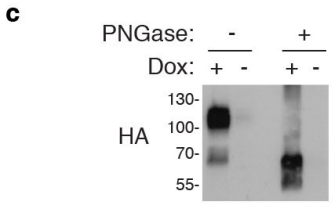

d

Bait	SLC38A9		SLC38A1		SLC38A2		SLC36A1	
Interactor	Sp. c.	Sq. c.	Sp. c.	Sq. c.	Sp. c.	Sq. c.	Sp. c.	Sq. c.
SLC38A9	36.5	30.5	0	0	0	0	0	0
SLC38A1	0	0	73.5	20.5	0	0	0	0
SLC38A2	0	0	0	0	65.5	15.0	0	0
SLC36A1	0	0	0	0	0	0	128.5	29.0
LAMTOR1	15.5	66.0	0	0	0	0	0	0
LAMTOR2	6.5	75.0	0	0	0	0	0	0
LAMTOR3	11.5	62.0	0	0	0	0	0	0
LAMTOR4	6.5	64.0	0	0	0	0	0	0
LAMTOR5	7.5	81.0	0	0	0	0	0	0
RAGA	19.5	45.0	0	0	0	0	0	0
RAGB	16.0	38.0	0	0	0	0	0	0
RAGC	23.5	45.0	0	0	0	0	0	0
RAGD	9.5	21.0	0	0	0	0	0	0

Extended Data Figure 3 | SLC38A9 proteomic analysis: bait localization and results. **a**, Single-channel and merged confocal microscopy images of DAPI stained nuclei and indirect immunofluorescence against HA-tagged SLC38A9 and endogenous lysosomal markers LAMP1 (top panel) and LAMP2 (middle panel) and the non-induced and secondary antibody only control (bottom panel) in HEK293 Flp-In TREx cells. Scale bar, 10 μm. Intensity profiles for SLC38A9 (green) and LAMP1, LAMP2 or secondary antibody control (red) along the cross-section lines indicated in the respective merged channel images are shown. **b**, Quantification of HA-SLC38A9 signal above background (dashed lines in **a**) that colocalizes with LAMP1, LAMP2 or secondary antibody only positive areas. Average and s.d. of at least two images is shown, analysing colocalization in 22, 34 and 27 cells respectively. **c**, HEK293 Flp-In TREx cells inducibly expressing SLC38A9 were treated or not with doxycycline (Dox) for 24 h. Where indicated, cell lysates were treated with PNGase and analysed by immunoblot. **d**, Tabular view summarizing the proteomic analysis of SLC38A9, SLC38A1, SLC38A2 and SLC36A1. Comparison of the SLC38A9 interactors identified by TAP–LC–MS/MS to the same analysis performed with the other transporters. Spectral counts (Sp. c., average of biological replicates) and sequence coverage (Sq. c., percentage, average of biological replicates) are indicated. Data shown are based on two independent experiments for each condition ($n = 2$), each analysed in two technical replicates.

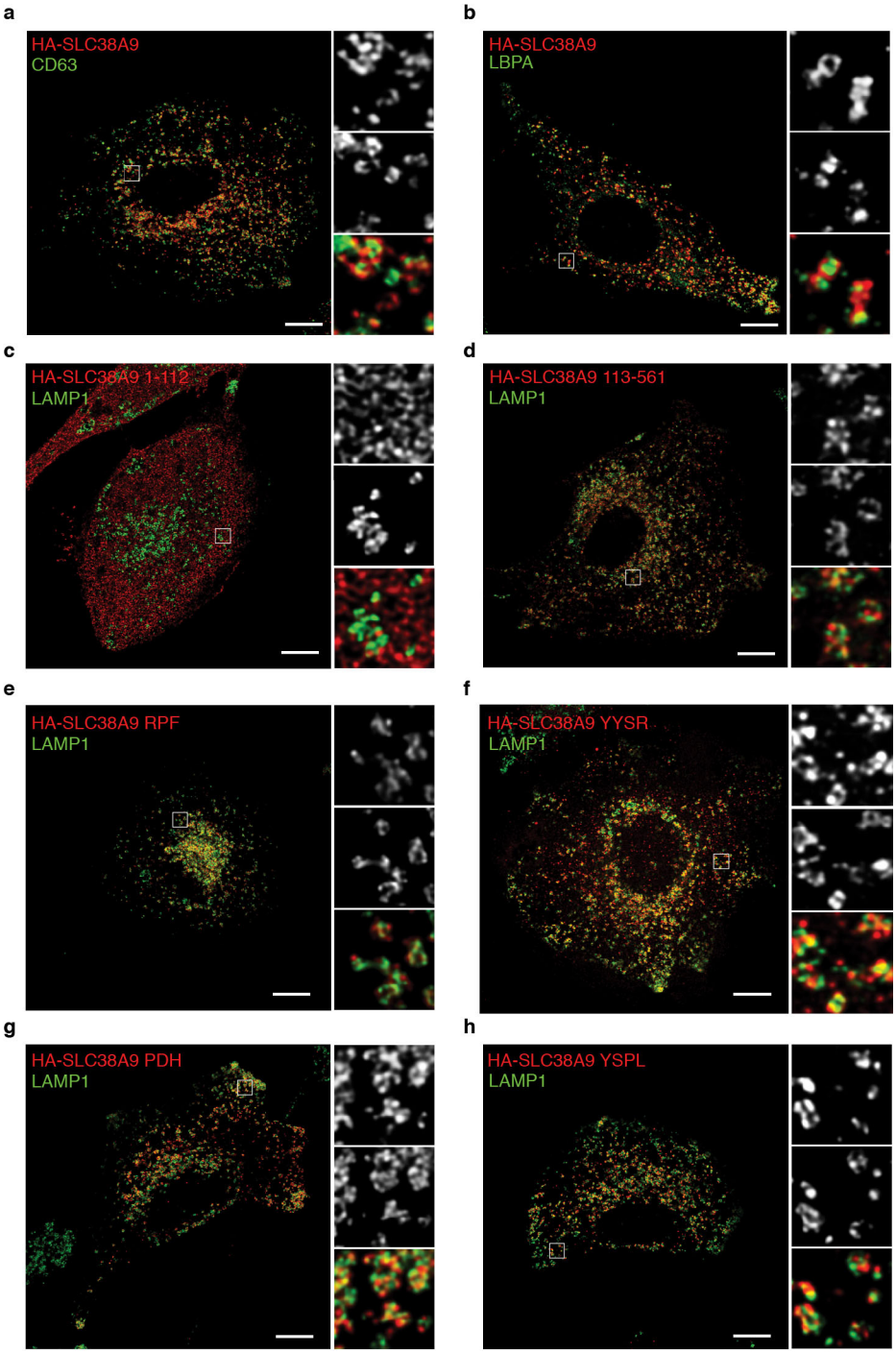

Extended Data Figure 4 | SLC38A9 localizes to the late endosome/lysosome compartment. **a–h**, HeLa cells were transfected with the indicated ST-HA tagged SLC38A9 construct. Merged and single-channel confocal microscopy images of indirect immunofluorescence of HA-tagged SLC38A9 (red) and endogenous lysosomal marker LAMP1 (green) are shown. Representative cells are shown. Scale bar, 10 μm.

a

Interactor \ Bait	LAMTOR1		LAMTOR3		LAMTOR4		LAMTOR5		RAGA		RAGC	
	Spec. count	Seq. cov.	Spec. count	Seq. cov.	Spec. count	Seq. cov.	Spec. count	Seq. cov.	Spec. count	Seq. cov.	Spec. count	Seq. cov.
SLC38A9	4.0	11.0	17.5	21.0	5.0	10.5	8.0	16.0	4.5	11.5	6.5	12.5
LAMTOR1	105.5	75.0	79.5	84.0	25.5	72.0	40.0	84.0	35.0	54.5	88.0	71.5
LAMTOR2	29.5	72.0	52.0	92.0	18.5	86.0	28.0	75.0	7.5	57.5	26.5	86.5
LAMTOR3	21.5	79.5	68.5	75.5	13.0	60.5	24.5	70.0	16.0	71.0	27.0	64.5
LAMTOR4	17.5	39.0	35.0	72.0	52.0	65.0	79.5	83.0	10.0	57.5	14.0	39.0
LAMTOR5	20.0	81.0	32.5	81.0	90.0	81.0	120.0	84.5	21.0	56.0	41.5	81.0
RAGA	31.0	42.5	67.5	64.5	21.0	39.5	25.0	47.5	145.0	56.0	82.0	51.5
RAGB	25.5	33.5	60.5	58.0	14.5	28.5	20.5	37.0	147.5	54.5	74.0	43.5
RAGC	34.5	45.5	81.5	64.5	19.0	42.0	28.5	55.5	52.5	44.5	202.5	62.0
RAGD	23.5	27.5	55.0	47.5	17.5	28.0	21.5	35.0	45.0	35.0	0	0
RAPTOR	9.0	8.0	31.5	24.5	11.5	10.0	18.5	15.5	5.0	5.0	3.0	3.0
ATP6V0D1	0	0	1.5	5.0	0	0	0	0	0	0	0	0
FNIP2	0	0	2.0	2.0	0	0	0	0	0	0	0	0
FLCN	0	0	4.5	11.0	0	0	0	0	0	0	0	0

b

LAMTORs_PD - SLC38A9 Peptide Mapping

```
MANMNSDSRH LGTSEVDHER DPGPMNIQFE PSDLRSKRPF CIEPTNIVNV NHVIQRVSDH 60
ASAMNKRIHY YSRLTTPADK ALIAPDHVVP APEECYVYSP LGSAYKLQSY TEGYGKNTSL 120
VTIFMIWNTM MGTSILSIPW GIKQAGFTTG MCVIILMGLL TLYCCYRVVK SRTMMFSLDT 180
TSWEYPDVCR HYFGSFGQWS SLLFSLVSLI GAMIVYWVLM SNFLFNTGKF IFNFIHHIND 240
TDTILSTNNS NPVICPSAGS GGHPDNSSMI FYANDTGAQQ FEKWWDKSRT VPFYLVGLLL 300
PLLNFKSPSF FSKFNILGTV SVLYLIFLVT FKAVRLGFHL EFHWFIPTEF FVPEIRFQFP 360
QLTGVLTLAF FIHNCIITLL KNNKKQENNV RDLCIAYMLV TLTYLYIGVL VFASFPSPPL 420
SKDCIEQNFL DNFPSSDTLS FIARIFLLFQ MMTVYPLLGY LARVQLLGHI FGDIYPSIFH 480
VLILNLIIVG AGVIMACFYP NIGGIIRYSG AACGLAFVFI YPSLIYIISL HQEERLTWPK 540
LIFHVFIIIL GVANLIVQFF M
```

c

SLC38A9_PD - SLC38A9 Peptide Mapping

```
MANMNSDSRH LGTSEVDHER DPGPMNIQFE PSDLRSKRPF CIEPTNIVNV NHVIQRVSDH 60
ASAMNKRIHY YSRLTTPADK ALIAPDHVVP APEECYVYSP LGSAYKLQSY TEGYGKNTSL 120
VTIFMIWNTM MGTSILSIPW GIKQAGFTTG MCVIILMGLL TLYCCYRVVK SRTMMFSLDT 180
TSWEYPDVCR HYFGSFGQWS SLLFSLVSLI GAMIVYWVLM SNFLFNTGKF IFNFIHHIND 240
TDTILSTNNS NPVICPSAGS GGHPDNSSMI FYANDTGAQQ FEKWWDKSRT VPFYLVGLLL 300
PLLNFKSPSF FSKFNILGTV SVLYLIFLVT FKAVRLGFHL EFHWFIPTEF FVPEIRFQFP 360
QLTGVLTLAF FIHNCIITLL KNNKKQENNV RDLCIAYMLV TLTYLYIGVL VFASFPSPPL 420
SKDCIEQNFL DNFPSSDTLS FIARIFLLFQ MMTVYPLLGY LARVQLLGHI FGDIYPSIFH 480
VLILNLIIVG AGVIMACFYP NIGGIIRYSG AACGLAFVFI YPSLIYIISL HQEERLTWPK 540
LIFHVFIIIL GVANLIVQFF M
```

Extended Data Figure 5 | SLC38A9 is an integral component of the Ragulator–RAG GTPase complex. **a**, Tabular view of spectral counts (Spec. count, average of biological replicates) and sequence coverage (Seq. cov., percentage, average of biological replicates) of the core Ragulator–RAG GTPase network and published interactors detected. Data shown are based on two independent experiments for each condition ($n = 2$), and analysed in two technical replicates. **b**, **c**, SLC38A9 peptides detected in LAMTOR1, 3, 4 and 5 (**b**) or in SLC38A9 (**c**) TAP–LC–MS/MS analysis are mapped on SLC38A9 sequence and highlighted in bold. Transmembrane helices are highlighted in light brown. Potential tryptic cleavage sites are in red.

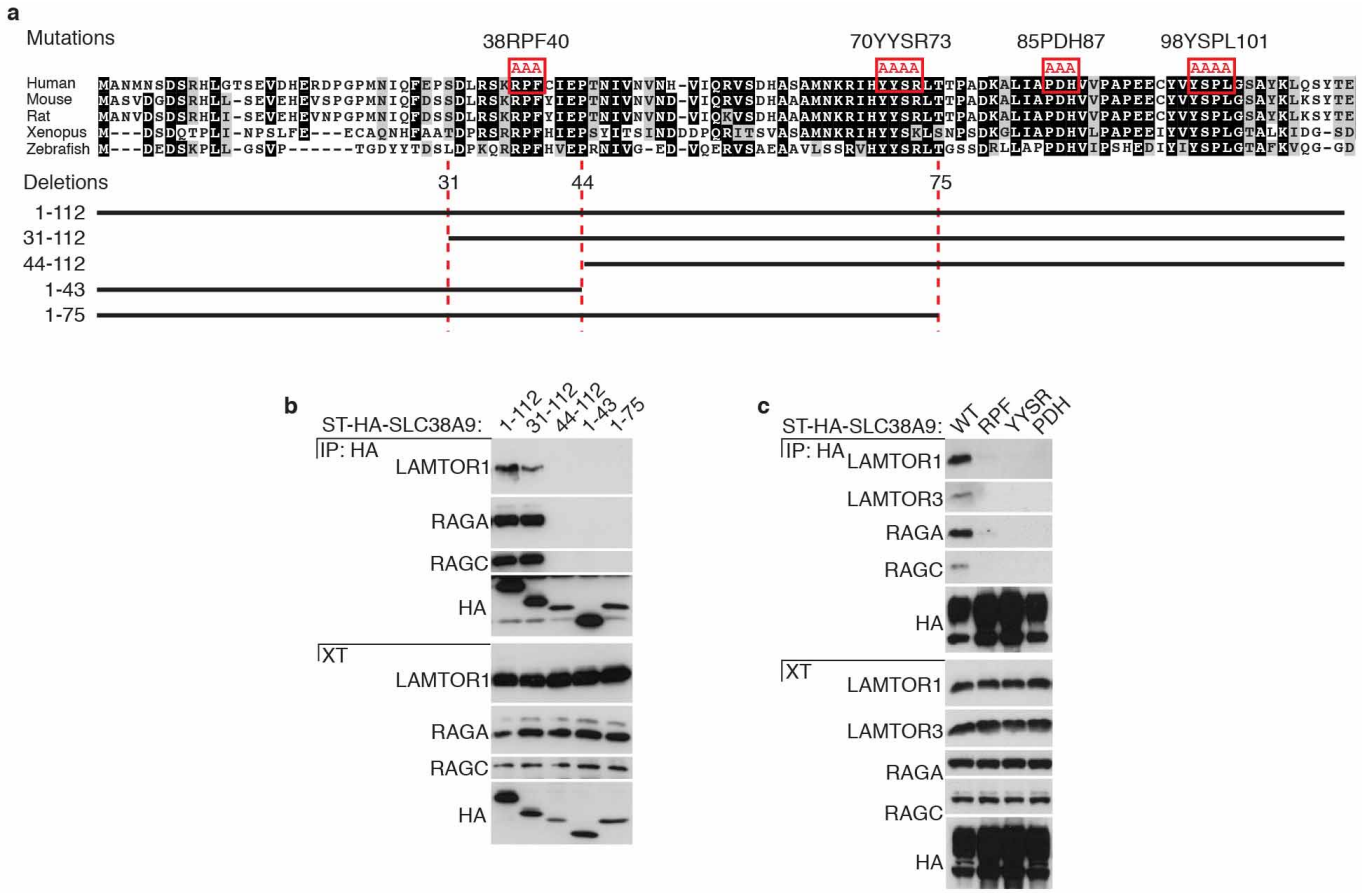

Extended Data Figure 6 | The cytoplasmic N-terminal region of SLC38A9 binds the Ragulator–RAG GTPase complex through evolutionary conserved motifs. **a**, Sequence alignment of the N-terminal cytoplasmic region (amino acids 1–112) of human, mouse, rat, *Xenopus* and zebrafish SLC38A9. Amino acids selected for deletion and motifs substituted to alanine are highlighted. Black and grey shading indicates >60% amino acid sequence identity and similarity, respectively. **b**, **c**, HEK293T cells were transfected with the indicated tagged SLC38A9 constructs. Immunoprecipitates and cell extracts were analysed by immunoblot. SLC38A9 mutant constructs are labelled with the number of the encoded amino acids (**b**) or with the amino acid motif substituted to alanine (**c**). Results are representative of two independent experiments ($n = 2$).

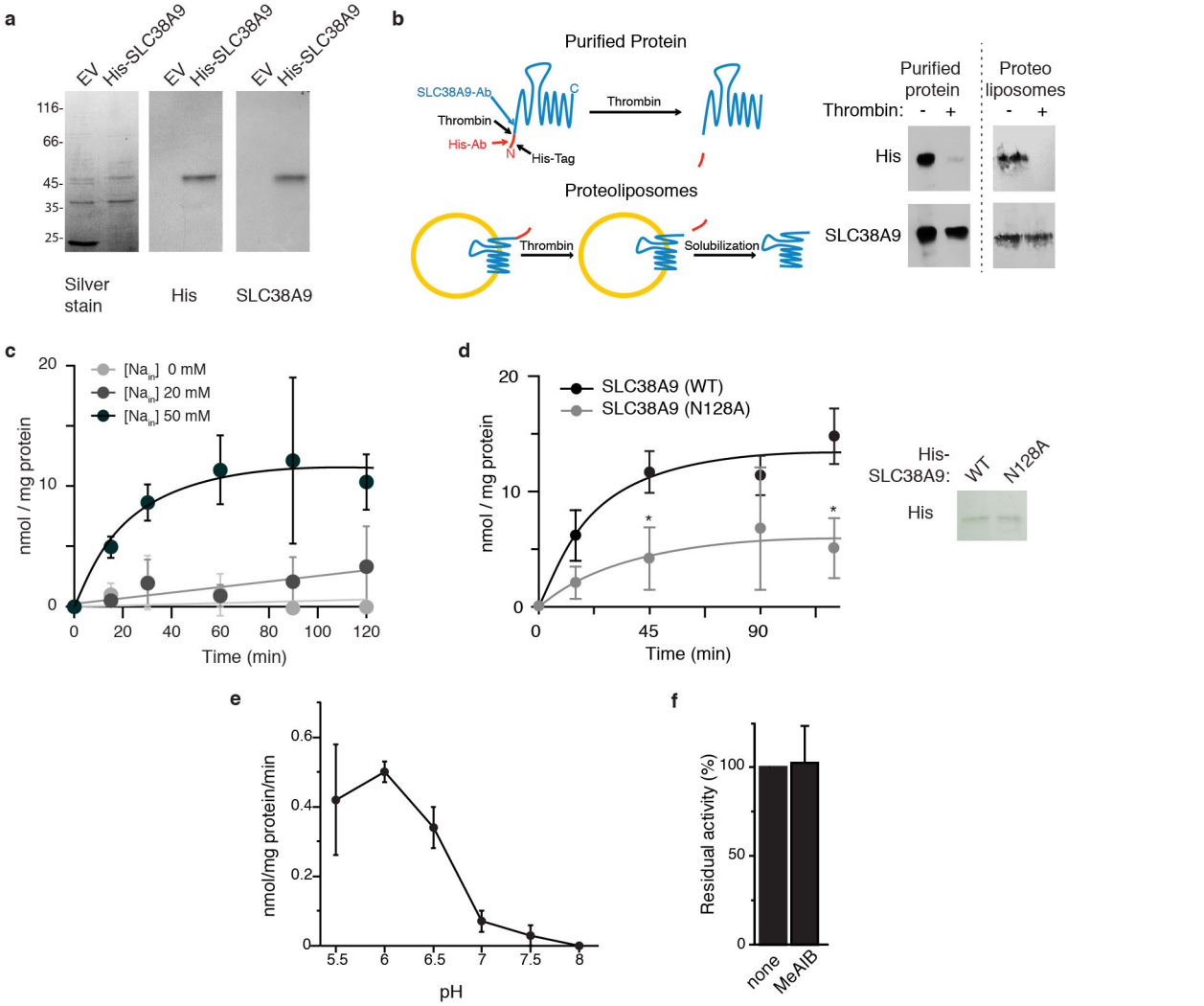

Extended Data Figure 7 | Characterization of SLC38A9-mediated amino acid transport in proteoliposomes. **a**, Purification of SLC38A9. Lanes represent empty vector control and SLC38A9 expressed in *E. coli* and purified by Ni-chelating chromatography. Immunoblot of the same fractions using anti-His or anti-SLC38A9 antibody are shown. **b**, Orientation of SLC38A9 in proteoliposomes. Purified His-SLC38A9 protein or proteoliposomes reconstituted with SLC38A9 were incubated overnight at 37 °C in presence or in absence of 1 U thrombin. Proteoliposomes were then solubilized with SDS and analysed by immunoblot. Results are representative of two independent experiments ($n = 2$). **c**, Time course of glutamine uptake by SLC38A9 in proteoliposomes reconstituted with the purified protein fraction. The uptake of 10 μM [^{3}H]glutamine was measured at different time intervals in the presence of the indicated intraliposomal sodium concentrations. Transport was calculated by subtracting the radioactivity associated to proteoliposomes reconstituted with the empty vector fraction. Values represent means of specific transport ± s.d. from three independent experiments ($n = 3$). **d**, Time course of glutamine uptake in proteoliposomes reconstituted with purified SLC38A9 wild-type or N128A mutant protein. Values represent means of specific transport ± s.d. from 3 independent experiments ($n = 3$). Significance was estimated by Student's *t*-test ($*P < 0.01$). Immunoblot analysis of purified protein reconstituted in the proteoliposomes. **e**, Effect of pH on the reconstituted SLC38A9. Reconstitution and transport assay were performed at the indicated pH. Results are means of specific transport rate ± s.d. from three different experiments ($n = 3$). **f**, Inhibition of the [^{3}H]glutamine uptake in proteoliposomes. 1 mM MeAIB (α-(methylamino)isobutyric acid) was added together with 10 μM [^{3}H]glutamine. Transport was measured at 60 min. Values represent means of percent residual activity with respect to control (without added inhibitor) ± s.d. from three independent experiments ($n = 3$).

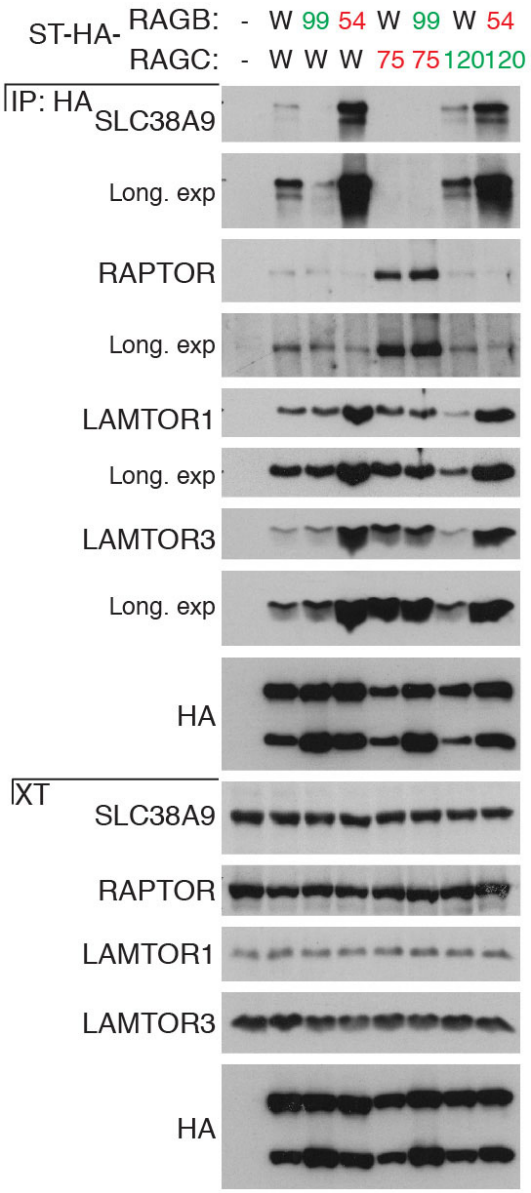

Extended Data Figure 8 | Nucleotide-loading/conformation dependent interaction of RAGB/RAGC heterodimers with SLC38A9. HEK293T cells were transfected with the indicated combination of tagged RAG GTPases mutant constructs or empty vector (−). Anti-HA immunoprecipitates and cell extracts were treated with PNGase and analysed by immunoblot. W, wild type; 75, S75N; 120, Q120L; 99, Q99L; 54, T54N. Results are representative of two independent experiments ($n = 2$).

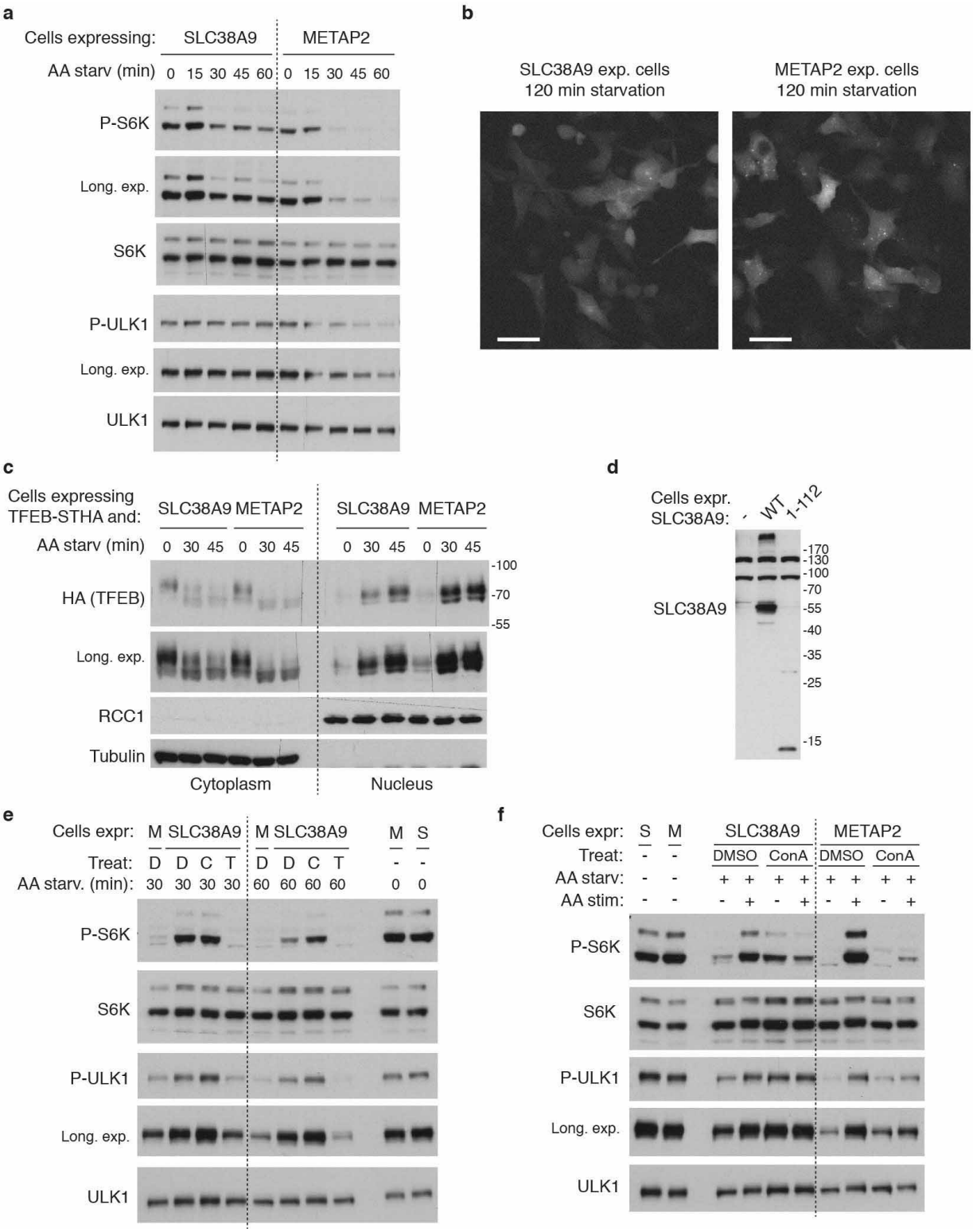

Extended Data Figure 9 | Stable expression of SLC38A9 mediates sustained mTORC1 activation upon amino acid starvation. **a**, SLC38A9 or METAP2 stably expressing HEK293T cells were starved for the indicated time in medium without amino acids and serum. Cell lysates were analysed by immunoblot. Results are representative of two independent experiments ($n = 2$). **b**, Representative images in the GFP channels of HEK293T cells stably expressing EGFP–LC3B and SLC38A9 or METAP2 starved for 120 min (related to Fig. 4b). Scale bar, 40 μm. **c**, HEK293T cells stably expressing TFEB–STHA and SLC38A9 or METAP2 were starved for the indicated time. Cytoplasmic and nuclear fraction were analysed by immunoblot. Results are representative of two independent experiments ($n = 2$). **d**, Immunoblot analysis of HEK293T cells stably expressing the indicated SLC38A9 constructs. **e**, SLC38A9 (S) or METAP2 (M) stably expressing HEK293T were starved for 50 min and then stimulated with amino acids for 20 min. Where indicated, cells were treated with concanamycin A (5 μM) or DMSO during both incubation times. Cell lysates were analysed by immunoblot with the indicated antibodies. Results are representative of two independent experiments ($n = 2$). **f**, SLC38A9 (S) or METAP2 (M) stably expressing HEK293T were treated for 30 min with DMSO (D), concanamycin A (C, 5 μM) or Torin 1 (T, 250 nM) and then starved for the indicated times in presence of the inhibitors. Cell lysates were analysed by immunoblot. Results are representative of two independent experiments ($n = 2$).

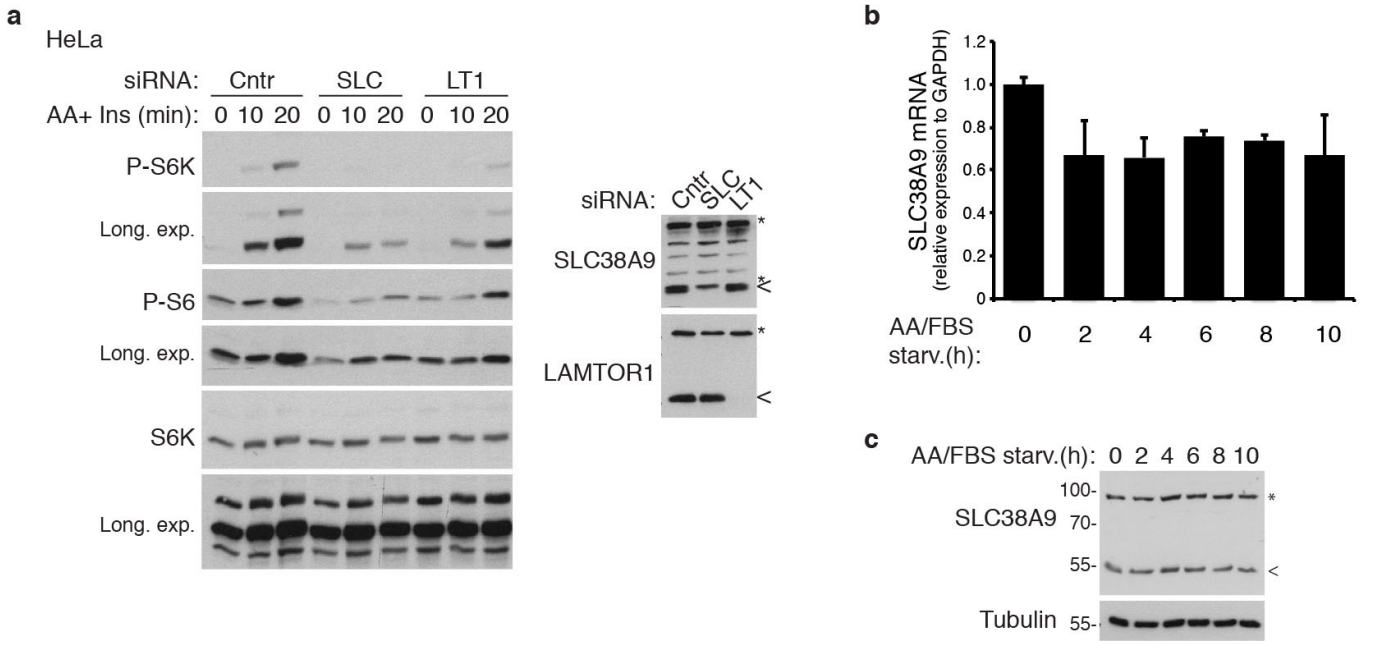

Extended Data Figure 10 | Expression of SLC38A9 is required for amino acid-induced mTORC1 activation and is not affected by starvation. **a**, HeLa cells were transfected with siRNA targeting SLC38A9 (SLC), LAMTOR1 (LT1) or non-targeting control (Cntr). After 72h, cells were starved for 50 min in medium without amino acids and serum and then stimulated with amino acids in presence of insulin (1 μM). Cell lysates were analysed by immunoblot. Results are representative of three independent experiments ($n = 3$). **b**, **c**, HEK293T cells were starved for the indicated times. SLC38A9 expression was analysed by quantitative PCR (**b**) and immunoblot (**c**). In **b**, mean values ± s.d. from technical triplicates are shown. Results are representative of two independent experiments ($n = 2$). <, SLC38A9; *, non-specific band.